UNIVERSITAT POLITÈCNICA DE VALÈNCIA

UNIVERSITAT POLITÈCNICA DE VALÈNCIA

School of Industrial Engineering

Study on the influence of reduction on three-dimensional porous sorbents based on graphene oxide for water treatment

Master's Thesis

Master's Degree in Industrial Engineering

AUTHOR: Kallen, Alexandre

Tutor: Pruna, Alina Iuliana

Cotutor: Giménez Torres, Enrique

ACADEMIC YEAR: 2023/2024

UNIVERSITAT POLITÈCNICA DE VALÈNCIA

ESCOLA TÈCNICA SUPERIOR ENGINYERIA INDUSTRIAL VALÈNCIA

UNIVERSITÉ DE LORRAINE

EEIGM
ÉCOLE EUROPÉENNE D'INGÉNIEURS EN GÉNIE DES MATÉRIAUX

Study of the influence of reduction on three-dimensional porous sorbents based on graphene oxide for water treatment

Master's Thesis

Alexandre Kallen

Tutor: Alina Iuliana Pruna

Co-Tutor: Enrique Giménez Torres

September 2023 – December 2023

Table of content

Table of figures

Table of tables

Abstract

Graphene aerogel (GAs) has emerged as a prominent material in the field of oil contamination research in recent years. Renowned for its exceptional properties, including extreme lightweight nature, high sorption capacity, and reusability, GAs have captured the attention of scientists for oil recovery applications. In this investigation, graphene oxide aerogels were synthesized through a hydrothermal approach. The study systematically explores the impact of various parameters, namely precursor concentration, freeze casting method, reducing agent, reducing agent amount, temperature, and thermal treatment on the oil sorption capacity of aerogels using engine, canola, and olive oils. Material morphology was characterized using SEM, and sorption properties were assessed through oil-in-water emulsion sorption experiments. Notably, a linear relationship between oil density and saturation sorption capacity was observed. The results indicate that the use of ethylenediamine as a reducing agent yielded better results compared to vitamin C, with the highest uptake reaching 405,24 mg/mg for an oil density of 1,471 mg/μL.

Keywords: Aerogel, graphene oxide, organic solvent absorption, oil spill recovery

Resumen

En los últimos años, el aerogel de grafeno (GA) se ha convertido en un material destacado en el campo de la investigación de la contaminación por petróleo. Conocidos por sus excepcionales propiedades, como su extrema ligereza, su alta capacidad de sorción y su reutilización, los aerogeles de grafeno han captado la atención de los científicos para aplicaciones de recuperación de petróleo. En esta investigación, se sintetizaron aerogeles de óxido de grafeno mediante un método hidrotérmico. El estudio explora sistemáticamente el impacto de diversos parámetros, a saber, la concentración de precursores, el método de liofilización, el agente reductor, la cantidad de agente reductor, la temperatura y el tratamiento térmico sobre la capacidad de sorción de aceite de los aerogeles utilizando aceites de motor, canola y oliva. La morfología del material se caracterizó mediante SEM y las propiedades de sorción se evaluaron mediante experimentos de sorción de emulsiones de aceite en agua. En particular, se observó una relación lineal entre la densidad del aceite y la capacidad de sorción de saturación. Los resultados indican que el uso de etilendiamina como agente reductor dio mejores resultados en comparación con la vitamina C, con una absorción máxima de 405,24 mg/mg para una densidad de aceite de 1,471 mg/μL.

Palabras clave: Aerogel, óxido de grafeno, absorción de disolventes orgánicos, recuperación de vertidos de petróleo.

I. Introduction

The need for sustainable and effective oil spill response strategies is ever more pressing in the face of an increasing threat to the environment from spills. Rapid developments in the relevant industries have been brought about by oil's extensive market demand. However, during oil exploitation, transport and processing the number of industrial activities has increased to such an extent that there is a high level of environmental pollution in particular with regard to oily wastewater.

Every year, approximately 5 million tonnes of oil are transported across the world's oceans, which poses a significant threat to marine life and ecosystems [1]. Water resources are seriously threatened by oil wastewater and its efficient treatment is an urgent environmental concern. However, the effect of common chemical dispersants used to control spills may have a further negative impact and lead to harm or shellfish mortality in certain cases [2].

Different techniques, including electrochemical, membrane based, biological, adsorption, and flotation methods, have been used for the treatment of oily wastewaters [3], [4], [5]. A rapid, efficient, and environmentally friendly approach to adsorption is emerging among these. Several materials, such as polypropylene, cellulose fiber, silkworm cocoon, raw cotton, or carbon-based materials, have been developed and utilized for their impressive adsorption performances [6], [7], [8].

Carbon based sorbents have received widespread attention over the past few years because of their special properties. Graphene aerogels, which have remarkable resilience and regenerative properties compared to traditional one- or two-dimensional materials, are particularly attractive for use in the separation of oil from water due to their exceptional sorption capacities [9], [10], [11], [12].

Graphene oxide or GO, which is a flexible material that serves as the basis for synthesis of 3D porous sorbents known as aerogels, has been found to be an excellent derivative of graphene. These aerogels are promising candidates for efficient oil absorption due to their specific porosity. The reduction process, a key step in synthesis, involves the removal of oxygen containing functional groups from GO and eventually turns it into graphene aerogel with enhanced properties for oil sorption. In this work, graphene oxide aerogels were synthesized via a hydrothermal reduction approach; the steps are shown in Figure 1.

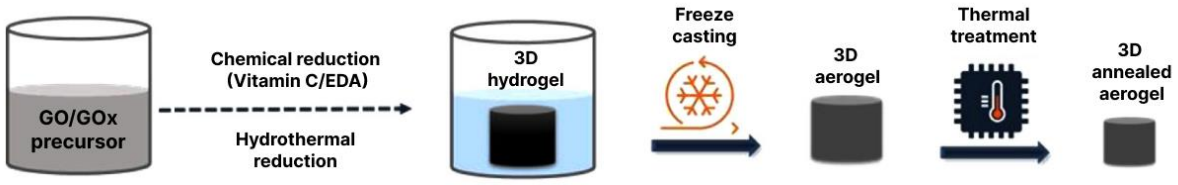

Figure 1: Synthesis of the GO aerogels via hydrothermal reduction approach [13].

The reduction of graphene oxide occurs through various mechanisms during the synthesis process, particularly through hydrothermal treatment. Two distinct approaches are usually employed: one involving vitamin C as a reducing agent and the other utilizing a molecule with amine groups, the ethylenediamine or EDA. Vitamin C acts by directly removing oxygen functional groups from GO, resulting in reduced graphene oxide. On the other hand, the amine-containing molecule indirectly reduces GO during hydrothermal synthesis by reacting with oxygen groups and introducing amine functionalities. These amine groups may function as spacers within the final aerogel, contributing to its unique porosity features.

The freeze-casting technique plays a pivotal role in defining the porosity of the aerogels. Freezing the hydrogel, obtained during the hydrothermal process, in liquid nitrogen or a conventional freezer affects the size and distribution of the pores. Subsequent lyophilization removes solvent ice crystals, leaving behind a porous structure mirroring the crystal formation. The choice of freezing conditions influences pore size and number, impacting the aerogel's sorption properties.

In hydrogel synthesis using the hydrothermal method, the precursor concentration significantly influences the resulting structure. Lower concentrations lead to increased dispersion of graphene oxide sheets, widening pores within the hydrogel. While this enhances porosity, it compromises the mechanical stability of the final aerogel monolith, affecting applications such as recycling and sorption processes.

The concentration of graphene oxide sheets in the original dispersion used for hydrogel synthesis influences the spatial arrangement and porosity of the resulting aerogel. Lower concentrations lead to better dispersion, reducing sheet stacking and resulting in wider pores. However, this may compromise the mechanical stability of the aerogel, impacting its suitability for sorption applications due to reduced re-usability.

Thermal annealing serves as a post-treatment method to further enhance reduction and modify the properties of graphene aerogels. In the case of vitamin C-based aerogels, annealing leads to an exfoliation of sheets, improving porosity and interconnection. For aerogels synthesized with amine-containing molecules, annealing removes amine groups, increasing the number of smaller interconnected pores.

This research not only examine the morphological changes resulting from reduction and post-treatments but also assesses the practical utility of these aerogels for oil sorption. The study considers various oils, including olive oil, canola oil, and engine oil, to analyze how oil density influences sorption performance.

This thesis seeks to fill the existing knowledge gap by conducting a comprehensive examination of how the mentioned synthesis parameters impact the morphological and absorption properties of three-dimensional porous sorbents based on graphene oxide. Additionally, the research aims to explain the connection between reduction-induced changes and the sorption efficiency of these aerogels concerning olive oil, canola oil, and engine oils. By exploring these relationships, this study seeks

to provide valuable insights for the advancement of environmentally friendly and effective strategies in oil spill remediation using advanced materials.

II. Materials and methods

1. Materials

The chemicals utilized in the experiment were of reagent grade and were obtained from Alfa Aesar, Sigma Aldrich in Valencia, Spain. These chemicals were used without any further modifications. Graphene oxide (GO) and expanded graphite oxide (GOx) aqueous slurries, containing GO nanosheets, were supplied by Graphenea in Donostia, Spain.

2. Synthesis of GO aerogels

The GO aerogels used in this work were prepared via a hydrothermal reduction. Several key parameters were varied to investigate their impact on the resulting aerogels.

During the aerogel synthesis, two distinct precursors, namely graphene oxide and exfoliated graphene oxide, were employed at concentrations spanning from 2 mg/mL to 0,5 mg/mL.

Subsequently, two distinct reducing agents were introduced: vitamin C, with a mass ratio of 1:2,5 relative to the precursor, and ethylenediamine, featuring mass ratios of 1:2,5.

The freeze-casting methodology was applied to the obtained hydrogel, with some samples subjected to conventional freezing at -20°C, On the other hand, one sample underwent immersion in liquid nitrogen, reaching the temperature of about -200°C.

A thermal treatment was administered to some aerogels, as post-synthesis treatment, involving exposure to 800°C for 1 hour under a nitrogen atmosphere.

These systematic variations in precursor, reducing agent, weight ratios, freeze-casting methods, and thermal treatment parameters constitute the main elements employed in this thesis to investigate the diverse characteristics of the synthesized aerogels.

Thus, GO aerogels were labelled following these abbreviations:

- GO for graphene oxide, GOx for exfoliated graphene oxide

- The subscript of GO/GOx (2, 1, 0.5) as their concentration in the dispersion to obtain the hydrogel and subsequently the aerogel
- VC for vitamin C and EDA for ethylenediamine as a reducing agent
- The subscript of VC/EDA 2.5 as the mass ratio of reducing agent/GO
- When the freezecast is performed in liquid nitrogen, * is used, otherwise its absence is used for freezecasting in conventional freezer
- TT when annealing is applied

So as an exemple:

- *"GO2VC2.5*_TT"* is the label for an aerogel using graphene oxide as its precursor with a concentration of 2mg/mL, with vitamin C as a reducing agent of 2.5:1 of mass ratio with respect to the graphene oxide, followed by freeze casting with liquid nitrogen and thermally treated (with annealing).

The synthesized aerogels and corresponding methods and parameters are summarized in Table 1**:** Synthesis parameters of each aerogel., for clarity and reference throughout the study.

Aerogel	Precursor	Reducing agent (w/w Ratio)	Freeze-casting	Thermal treatment (Annealing)
GO2VC2.5_TT	2 mg/mL GO	1:2.5 VC	Freezer (-20°C)	TT (800°C 1h; N_2)
GO2VC2.5*_TT	2 mg/mL GO	1:2.5 VC	Liquid N (-200°C)	TT (800°C 1h; N_2)
GOx1VC2.5	1 mg/mL GOx	1:2.5 VC	Freezer (-20°C)	No TT
GOx1VC2.5_TT	1 mg/mL GOx	1:2.5 VC	Freezer (-20°C)	TT (800°C 1h; N_2)
GOx0.5VC2.5	0.5 mg/mL GOx	1:2.5 VC	Freezer (-20°C)	No TT
GOx0.5VC2.5_TT	0.5 mg/mL GOx	1:2.5 VC	Freezer (-20°C)	TT (800°C 1h; N_2)
GO2EDA2.5_TT	2 mg/mL GO	1:2.5 EDA	Freezer (-20°C)	TT (800°C 1h; N_2)
GOx1EDA2.5	1 mg/mL GOx	1:2.5 EDA	Freezer (-20°C)	No TT
GOx1EDA2.5_TT	1 mg/mL GOx	1:2.5 EDA	Freezer (-20°C)	TT (800°C 1h; N_2)

Table 1: Synthesis parameters of each aerogel.

3. Material characterization

A. Physical characteristics of aerogel sorbents

The aerogel dimensions were measured with a calliper with accuracy 0,05 mm (measurement error is estimated as ±10%).

The aerogel weight was measured using a KERN 700 balance (with a precision of ±0,01mg).

The apparent density of the aerogels was calculated by dividing their weight to their volume.

Then, using their apparent density, the porosity and the pores volume were calculated as follows:

$$\eta\ (\%) = \left(1 - \frac{\rho_{aerogel}}{\rho_{graphite}}\right) * 100\% \quad (1)$$

$$V_{pores}\ (cm^3/mg) = \frac{1}{\rho_{aerogel}} - \frac{1}{\rho_{graphite}} \quad (2)$$

Where η is the porosity of the aerogel (%), $\rho_{aerogel}$ is the apparent density of the aerogel (mg/cm^3) and $\rho_{graphite}$ is the density of graphite, taken as 2200 mg/cm3 [14], [15].

B. Surface properties of aerogel sorbents

The surface morphologies of the aerogels were obtained using a scanning electron microscope (Zeiss GeminiSEM 500-8203017153 displayed on Figure 2).

Figure 2: Zeiss Gemini 500 FESEM in Gaithersburg, USA [16].

In conventional scanning electron microscopy (SEM) systems, the surface of a solid sample is excited with a highly focused energetic beam of electrons which induces X-ray fluorescence from the elements within the sample. Samples must be run under high vacuum conditions and must be conductive or coated with a conducting material such as gold for proper analysis. X-ray microanalysis of uncoated non-conductive samples in the conventional SEM is hampered by specimen charging which can reduce the energy of the electron beam and make quantitative analysis impossible.

The set-up of a common SEM is shown in Figure 3. An electron beam is generated in the electron gun. While traveling in the column the beam is formed and

focused by various electromagnetic lenses and deflection coils. The sample is located in a chamber and the electron beam is scanned over the surface of the specimen. The electrons hit the specimen and interact with it. The resulting electrons are detected [17].

The detected electrons are used to create an image. It can be differed between two operation principles. Either secondary or backscattered electrons can be detected. Figure 3 shows the interaction volume that results from the electron beam hitting the specimen and where the detected electrons come from.

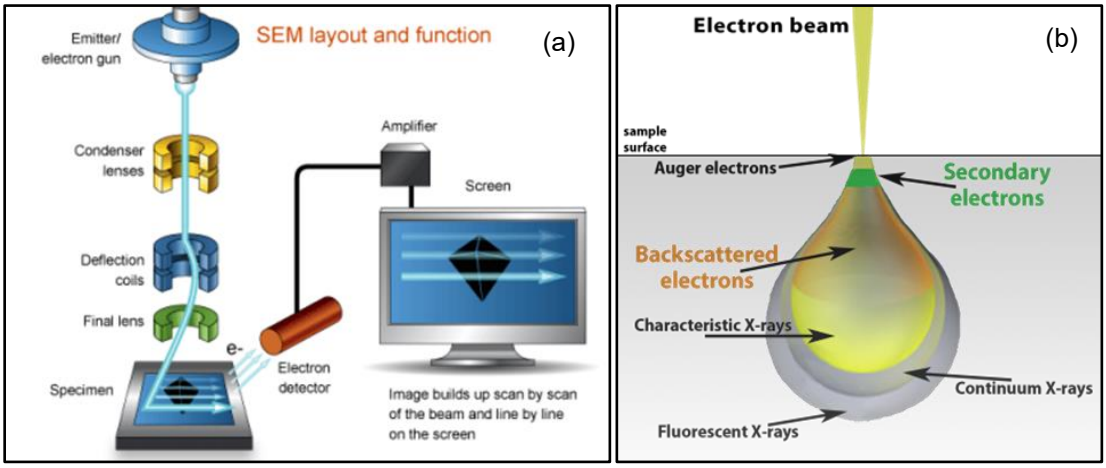

Figure 3 : Principle of a scanning electron microscope (a) [17], Interaction of the electron beam with the material (b) [18].

As shown, secondary electrons are from the specimen surface. These originate from the material itself when the beam is hitting the surface. In contrast, the backscattered electrons are electrons from the beam. These interact with the material, are scattered back, and detected. Depending on the operation mode used, different information can be obtained. Secondary electrons mainly provide information about the topography but also of the morphology. When working with a backscattered electron detector the topography can also be examined. Besides, the composition and crystallinity of the specimen can be investigated [19].

4. Sorption performance of graphene aerogels

To assess the sorption properties of graphene aerogels, specifically the oil gravimetric sorption capacity (expressed as mass of sorbed oil per mass of dry sorbent material, and denoted as Qg), three representative oils were employed in this investigation. These oils included canola oil with a density of 1,472 g/cm³, extra virgin olive oil with a density of 1,126 g/cm³, and motor oil 5W-40 with a density of 0,888 g/cm³.

In order to record the kinetics of absorption, a cut piece of graphene aerogel was carefully placed in a beaker containing 25 mL of distilled water. Then, incremental volumes of oil, ranging from 5 µL to 20 µL, were meticulously dropped on the aerogel using a micropipette (Micropipette Research plus Eppendorf, as depicted in Figure 4).

This sorption methodology was designed to mitigate the influence of water sorption on the oil sorption performance This methodological choice is based in the principle that aerogels, possessing high porosity and surface area, tend to exhibit an inherent affinity for moisture absorption. By pre-soaking the aerogel in distilled water, the available surface sites on the aerogel are saturated with water molecules, reducing the likelihood of subsequent water sorption during the oil sorption phase.

Water, being a highly polar molecule, can compete with non-polar oils for sorption sites on the aerogel surface. If the aerogel were not pre-saturated with water, there could be a higher probability of water molecules occupying these sites during the initial stages of the oil sorption experiment, potentially impacting the accuracy of the observed oil sorption capacity. The pre-soaking step with distilled water effectively minimizes this interference, allowing the subsequent oil sorption measurements to more accurately reflect the aerogel's capacity to absorb and retain oil. Therefore, this controlled approach enhances the precision and reliability of the experimental data.

For a better visualization of the absorption process, a red dye was added to all oils.

The duration for the aerogel to absorb each incremental volume of oil was recorded, and the process was iterated until saturation was reached, indicated by a visible red halo around the aerogel thanks to the dye (as illustrated in Figure 4).

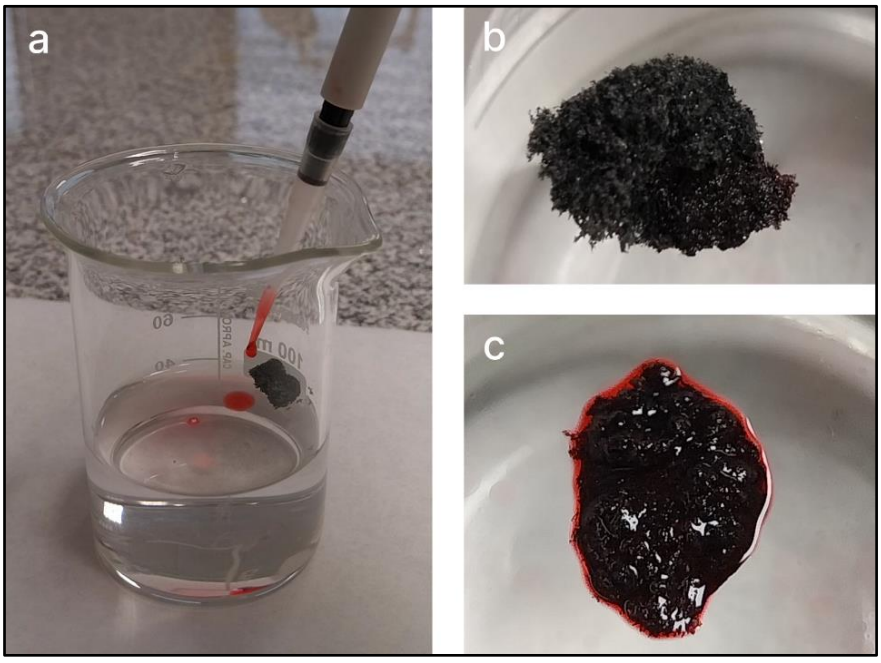

Figure 4: Experimental procedure (a), GOx1VC2.5_TT at the start of sorption experiment (b), GOx1VC2.5_TT at the end of the sorption experiment, saturation showed with a red halo (c).

All experiments were conducted at a constant room temperature of 24°C, with the exception of two kinetics absorption experiments for GOx1EDA2.5_TT and GOx1VC2.5_TT. In these experiments, the beaker containing distilled water and oils were placed on a hot plate, elevating the temperature to 60°C, thereby enabling an investigation on the impact of temperature on sorption capacity. Given that the sorption measurements are fast, kinetics being recorded for the order of seconds.

5. Analysis

After performing the sorption experiments, all data were collected and processed on Microsoft Excel.

From the quantity of oil increments and their density, we can then determine the mass of oil absorbed by the aerogel and thus calculate the gravimetric sorption capacity, the sorption rate and the pore volume occupancy as follows:

$$Q_g\ (mg/mg) = \frac{Total\ m_{oil\ absorbed}}{m_{aerogel}} = \frac{Total\ V_{oil\ absorbed} * \rho_{oil}}{V_{aerogel} * \rho_{aerogel}} \quad (3)$$

$$SR\ ((mg/mg)/s) = \frac{Q_g}{Total\ absorption\ time} \quad (4)$$

$$Pore\ volume\ occupency\ (\%) = \frac{Total\ V_{oil\ absorbed}}{V_{pores} * m_{aerogel}} * 100\% \quad (5)$$

The results were then plotted as shows Figure 5. Close examination of the kinetic curve revealed a well-defined logarithmic trend, characterized by rapid initial growth followed by gradual stabilization.

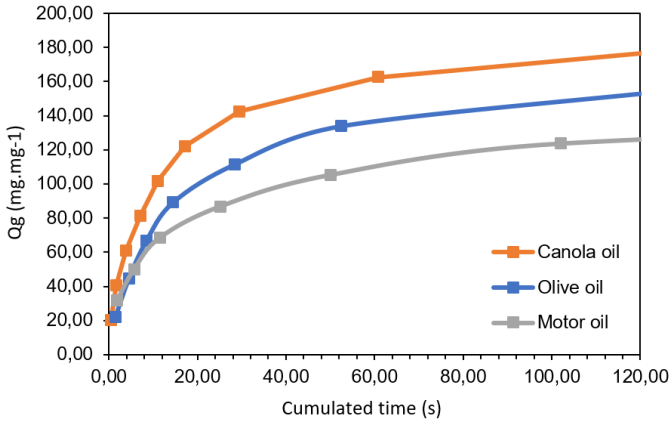

Figure 5: Kinetics sorption curve of GO2VC2.5_TT.

In most of the experiments, saturation was found to peak at around 100 to 120 seconds. In order to ensure a standardized comparison between the different curves,

the data was collected at a specific point in time, *i.e.* at 120 seconds. This approach is intended to allow a fair assessment of performance between the different data sets, thus assuring the coherence of the results.

III. Results and discussion

1. Morphology

The initial examination involved SEM observation. Surface morphologies of GO aerogels submitted to different synthesis parameters were analyzed with SEM microscope and are displayed on Figure 6.

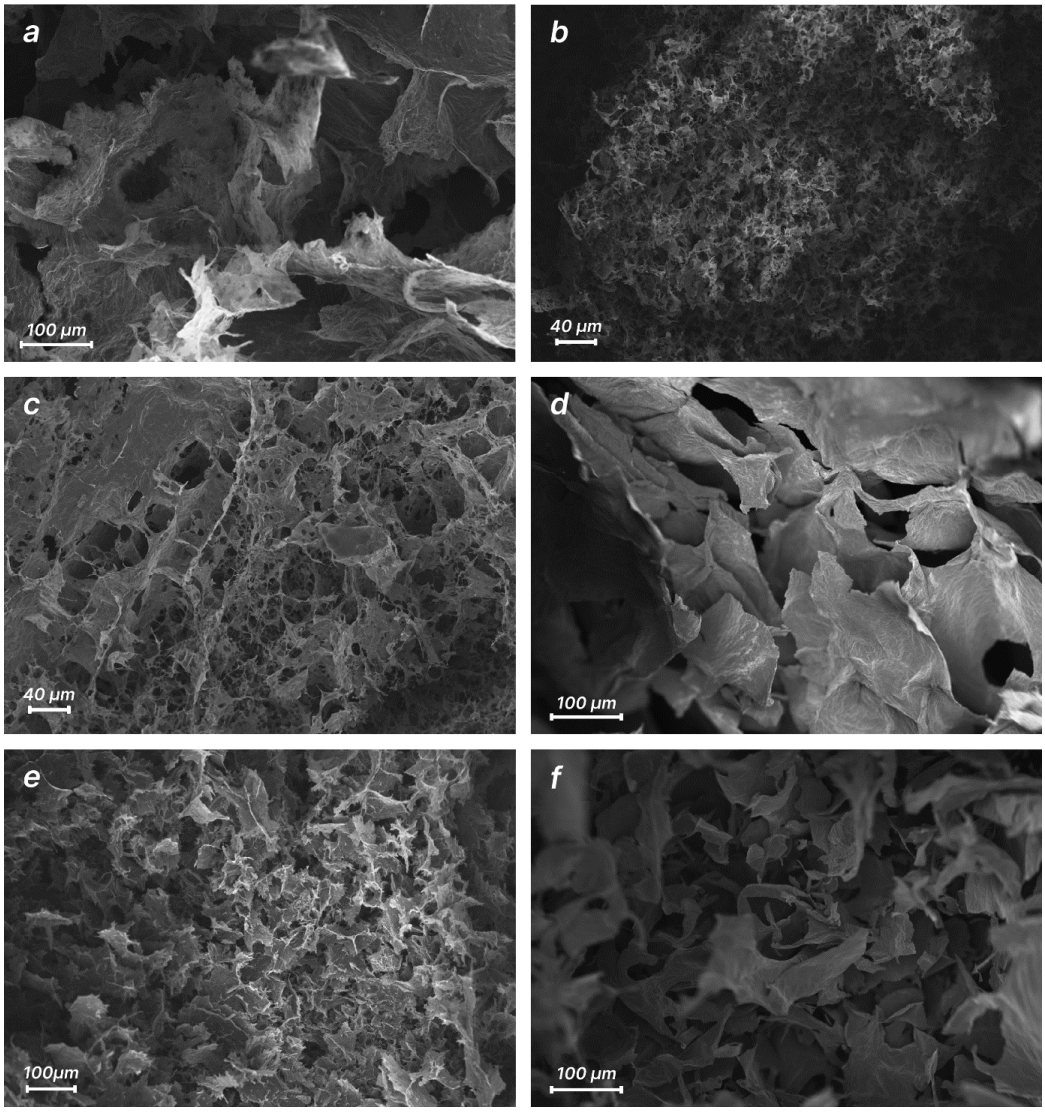

Figure 6: SEM images of GO aerogels as a function of reducing agent and freeze casting medium and thermal post-treatment (TT): a) VC + freezer; b) VC + liquid nitrogen; c) EDA + freezer; d) VC + freezer + TT; e) VC + liquid nitrogen + TT and f) EDA + freezer + TT

First, it should be noted that all aerogels exhibit a highly porous interconnected three-dimensional structure.

The morphological influence of freeze casting can be seen on Figure 6a for conventional freezer and Figure 6b for liquid nitrogen, where the aerogel that was submitted to the conventional freezer exhibit a thick random oriented sheets microstructure with large pores whereas for the liquid nitrogen, the aerogel tends to exhibit a thin cellular microstructure with a more numerous but smaller pores. This result may be attributed to the change in the ice crystal shape of during the solidification process [20], [21].

During this process in freeze casting, two coexisting phases are taking place, nucleation, and the growth of the ice crystals. For ice nucleus to form, the liquid needs to reach an activation energy, transitioning from a disordered, less stable state (water) to a more ordered, more stable state (ice).

At fast solidification rate (-200°C in liquid nitrogen) this activation energy is easier to reach, enabling formation of numerous ice nuclei. However, crystal growth is limited due the scarcity of available liquid water because of the high number of crystals growing at the same time. After the removal of the ice phase via sublimation, this yields a numerous yet small pores, as shown in Figure 6b.

At a slow solidification rate (-20°C), the activation energy is harder to reach, enabling only few crystal nuclei to appear. However, those nuclei will have lot of available liquid water to grow and then form few yet big pores after sublimation as shown in Figure 6a and Figure 7.

At a slow solidification rate (-20°C), the activation energy is harder to reach, enabling only few crystal nuclei to appear. However, those nuclei will have lot of available liquid water to grow and then form few yet big pores after sublimation as shown in Figure 6a and Figure 7.

This phenomenon is also supported by Figure 8, displaying the density and pore volume with respect to the freeze casting method. It shows that a higher pore volume is formed during a freezing at -20°C than at -200°C, also the density is inversely proportional to the pore volume, the pores being close packed. The density is lower during a freezing at -200°C then at -20°C. Also, the role of ice crystals and GO content in determining the wall thickness of graphene aerogels is significant.

A reduction in the size of ice crystals is associated with a decrease in GA wall thickness, whereas an increase in GO content results in an increase in wall thickness. The formation of numerous ice crystals contributes to the reduction in wall thickness [22]. Therefore, liquid nitrogen freeze casting yields thinner walls compared to conventional freezer casting technique.

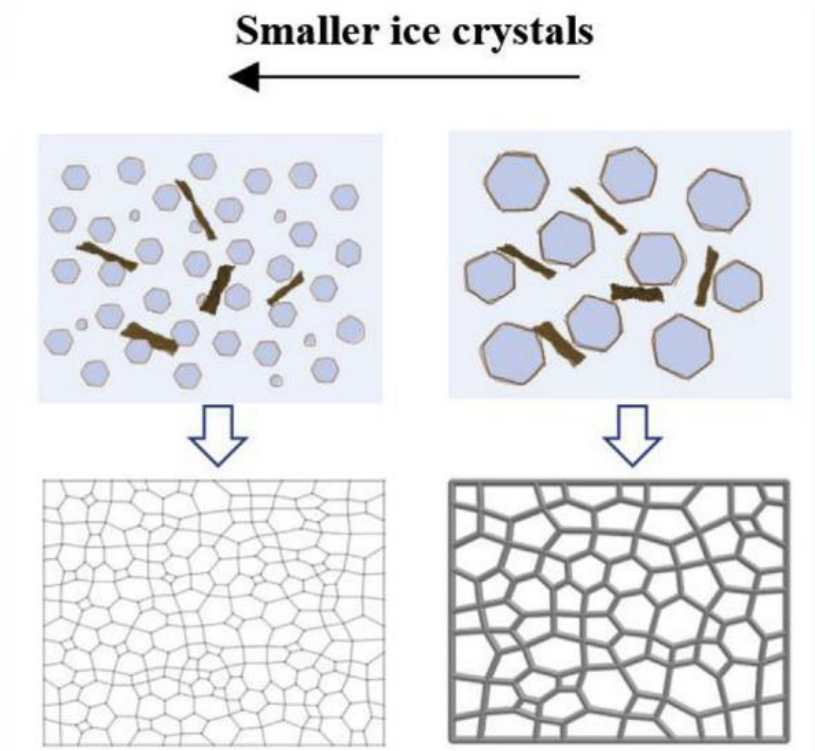

Figure 7: Illustration of the effect of the size of ice crystals on the wall thickness and pore size [22].

The impact of the reducing agent on the microstructure is shown in Figure 6a and Figure 6c with respectively VC and EDA. As mentioned before, the microstructure of the aerogel reduced with VC in Figure 6a exhibits big, coarse, and random oriented sheets whereas the aerogel reduced with EDA shows more of a smaller uniform, cellular microstructure but with rougher surface than Figure 6b. The effects on pores volume and density are shown in Figure 8. When reduced with EDA, the aerogel has a lower density and a bigger pore volume compared to the one reduced with VC.

Finally, the effect of annealing can be assessed through the comparison of Figure 6a, Figure 6b and Figure 6c compared to respectively Figure 6d, Figure 6e and Figure 6f. When annealed, the surface morphology appears smoother, especially for an EDA sample, where bigger smoothed sheets are formed, also yielding bigger pores, as seen on Figure 6f. For VC freeze-casted at -20°C, the morphology is changed into some more layered, organized sheets, displayed on Figure 6e.

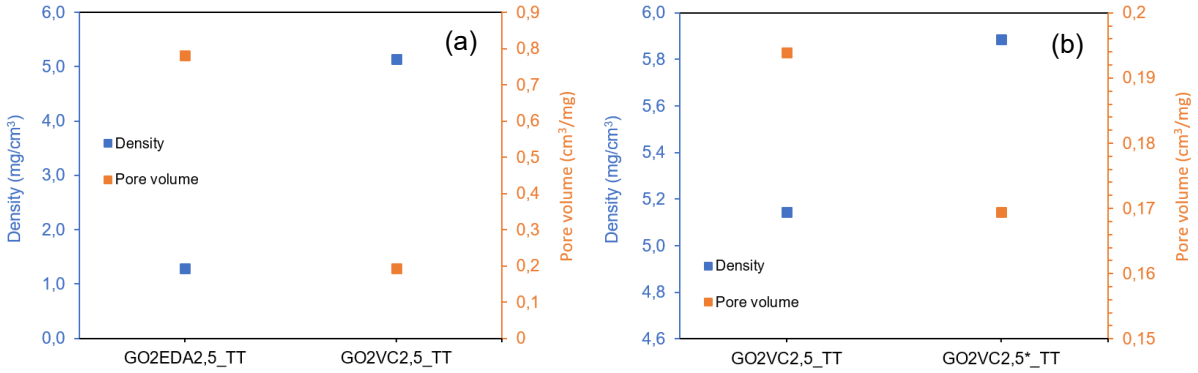

Figure 8: Evolution of density and pore volume for GO2EDA2.5_TT and GO2VC2.5_TT (a), evolution of density and pore volume for GO2VC2.5_TT and GO2VC2.5*_TT (b).

2. Absorption performance

In this section, an examination of several crucial parameters that influence the performance of GO aerogel in this thesis will be performed. In particular, a look at the initial GOx concentration, the annealing, the freeze casting method, the choice of reducing agent, and the sorption process temperature will be done. These factors have been identified as key determinants, each playing a specific role in the morphology and final properties of the aerogel. By understanding the individual influence of these parameters, the aim is to provide in-depth insights into optimising the performance of GO aerogel.

A. Effect of annealing

Annealing, a thermal treatment method that involves heating a material to a specific temperature and holding it there for a predetermined time, followed by controlled cooling, plays a pivotal role in modifying the structural and chemical properties of GO aerogels, consequently influencing their sorption capacities.

From the Figure 9a, the sorption capacity (respectively sorption rate) of non-annealed aerogels compared to annealed ones are as follows:

From 85,32 mg/mg (0,67 (mg/mg)/s) to 193,57 mg/mg (1,44 (mg/mg)/s) for canola oil; from 56,91 mg/mg (0,49 (mg/mg)/s) to 160,87 mg/mg (1,40 (mg/mg)/s) for olive oil and from 45,18 mg/mg (0,34 (mg/mg)/s) to 124,40 mg/mg (0,97 (mg/mg)/s) for motor oil.

Therefore, the values show a clear trend of increasing sorption capacity and sorption rate values with the presence of annealing. Also, for the results of the different

oil of the same aerogel, the higher the density, the higher the sorption and sorption rate. In this the case for all the test that have been done on the aerogels.

From the Figure 9b, the pore occupancy (respectively ratio to the total volume) of non-annealed aerogels compared to annealed ones are as follows:

From 0,057 cm^3/mg (16%) to 0,130 cm^3/mg (32%) for canola oil, from 0,051 cm^3/mg (14%) to 0,143 cm^3/mg (34%) for olive oil and from 0,051 cm^3/mg (14%) to 0,139 cm^3/mg (33%) for motor oil.

Therefore, the pore occupancy of the oil displays the same trend, increasing with the presence of annealing. Moreover, it is important to note that aerogel submitted to annealing have not only better pore occupancy by the oil but also a bigger pore volume.

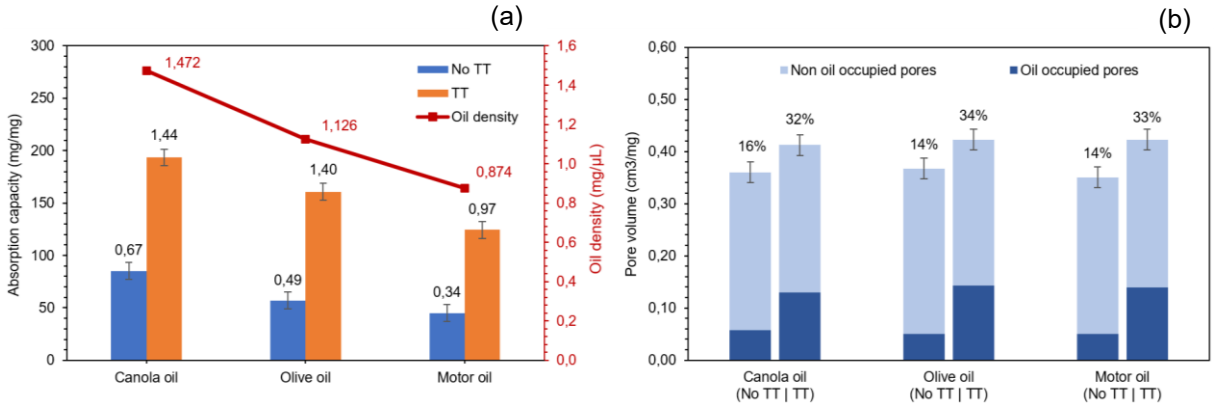

Figure 9: Study of the annealing influence by comparison of sorption capacity and sorption rate ((mg/mg)/s, values indicated in the plot) between GOx0.5VC2.5 and GOx0.5VC2.5_TT for different oils (a), comparison of the pore volume occupied by the oil (percentage of total volume indicated in the plot) between GOx0.5VC2.5 and GOx0.5VC2.5_TT (b).

From the Figure 10a, the same trend on the increase of sorption capacity and sorption rate value with the presence of annealing can be observed, similarly to Figure 9a. The sorption capacity for canola oil (respectively sorption rate) of non-annealed aerogels compared to annealed ones are as follows:

From 39,62 mg/mg (0,33 (mg/mg)/s) to 165,88 mg/mg (1,50 (mg/mg)/s) between GOx1VC2.5 and GOx1VC2.5_TT; from 85,32 mg/mg (0,67 (mg/mg)/s) to 193,57 mg/mg (1,44 (mg/mg)/s) between GOx0.5VC2.5 and GOx0.5VC2.5_TT and from 169,23 mg/mg (1,22 (mg/mg)/s) to 191,45 mg/mg (1,60 (mg/mg)/s) between GOx1EDA2.5 and GOx1EDA2.5_TT.

From the Figure 10b, also the same trend on increased oil occupied pores can be observed as in Figure 9b. The increasing canola oil pore occupancy (respectively ratio to the total volume) of non-annealed aerogels compared to annealed ones are as follows:

From 0,027 cm^3/mg (12%) to 0,111 cm^3/mg (56%) between GOx1VC2.5 and GOx1VC2.5_TT; from 0,057 cm^3/mg (16%) to 0,130 cm^3/mg (32%) between GOx0.5VC2.5 and GOx0.5VC2.5_TT and from 0,090 cm^3/mg (14%) to 0,129 cm^3/mg (16%) between GOx1EDA2.5 and GOx1EDA2.5_TT.

Moreover, except between GOx1VC2.5 and GOx1VC2.5_TT which shows almost the same pore volume, is important to note that aerogel submitted to annealing have not only better pore occupancy by the oil but also a bigger pore volume.

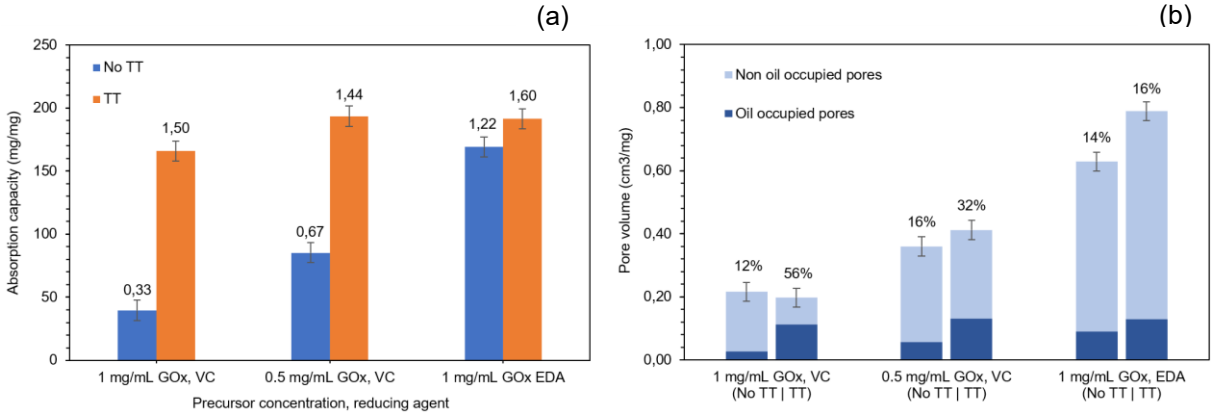

Figure 10: Study of the annealing influence by comparison of sorption capacity and sorption rate ((mg/mg)/s, values indicated in the plot) between GOx1VC2.5 and GOx1VC2.5_TT, GOx0.5VC2.5 and GOx0.5VC2.5_TT, GOx1EDA2.5 and GOx1EDA2.5_TT for canola oil (a), comparison of the pore volume occupied by canola oil (percentage of total volume indicated in the plot) between GOx1VC2.5 and GOx1VC2.5_TT, GOx0.5VC2.5 and GOx0.5VC2.5_TT, GOx1EDA2.5 and GOx1EDA2.5_TT (b).

On a more theoretical basis, the main role of annealing is to reduce the GO aerogel, as the graphene oxide is a highly oxidized form of graphene, containing numerous oxygen function groups such as hydroxyl, epoxy, or carboxyl groups. Therefore, when put in a reducing atmosphere, such as the nitrogen used in this thesis, annealing will lead to the removal of those oxygen functional groups, following multiples steps as shown in Figure 11.

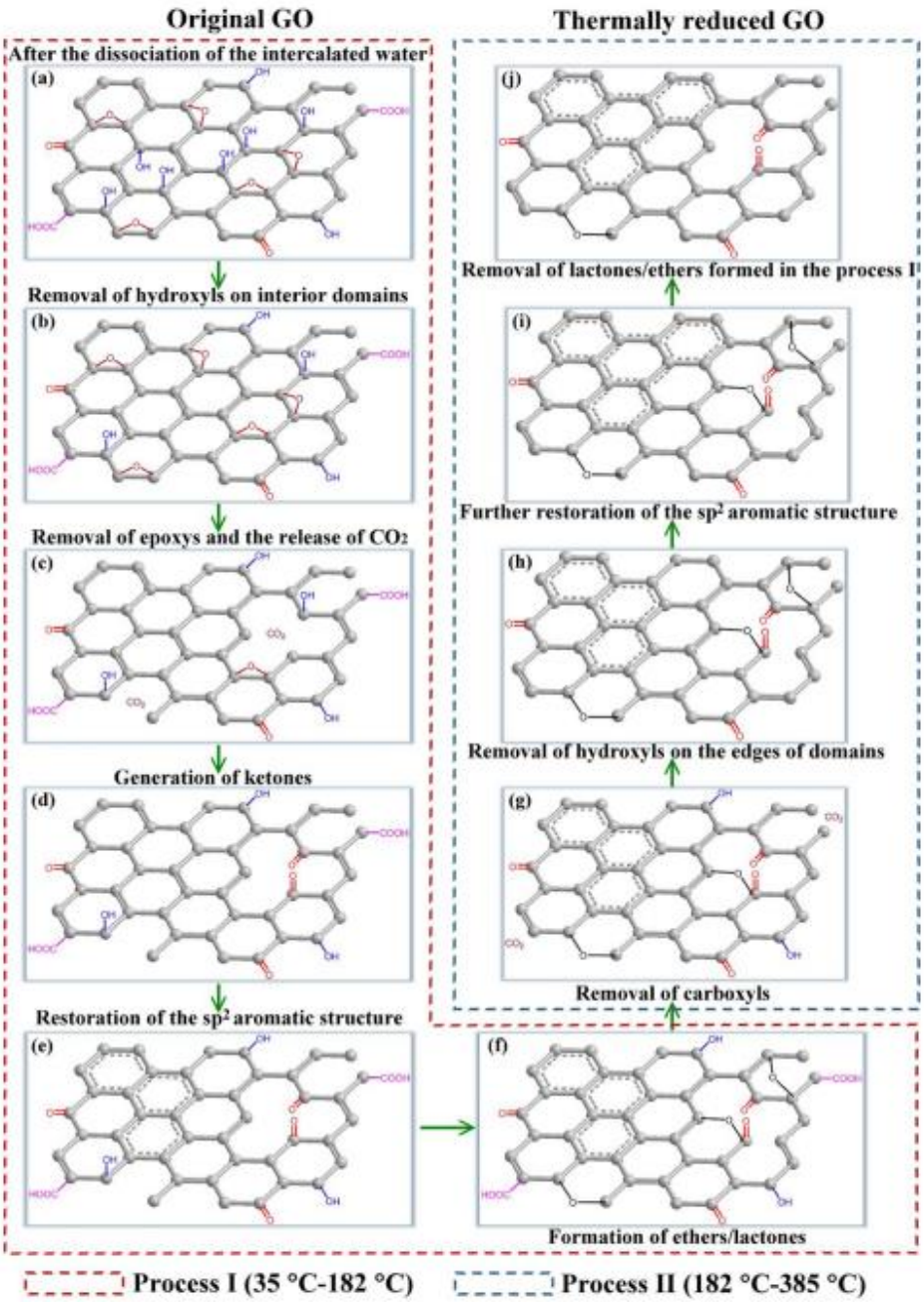

Figure 11: Illustration of the multiple steps of GO oxygen groups reduction depending on temperature [23].

The presence of oxygen in the GO aerogel introduces polar functional groups that creates hydrogen bonding and electrostatic interactions with water molecules. This leads to increased hydrophilicity, improving the uptake and retention of water within the aerogel pores. Therefore, the removal of oxygen through annealing results in reduced affinity for water and enhanced hydrophobicity.

The temperature of annealing plays an important role in the reduction process. Kumar P. and al. (2023) found that annealing the aerogel at a temperature of 400 °C resulted in minimal composition changes. However, elevating the annealing

temperature to 750 °C increased the carbon content to 96%, while reducing oxygen to 4%, compared to the initial 89% of carbon content to 11% of oxygen content. At a temperature of 1300°C, the graphene aerogel exhibited over 99,4% carbon and less than 0,6% oxygen content. The complete removal of oxygen was only achieved when annealing the graphene aerogel reached 2700 °C. [24]

Moreover, the breaking of C-O bonds is accompanied by a consequential transformation of the carbon lattice structure. Initially, the carbon atoms in graphene oxide are often in a sp3 hybridized state, forming tetrahedral structures. The removal of oxygen atoms during annealing creates vacancies in the lattice and leaves behind unsaturated carbon sites. Also, these breaking of C-O bonds can led to C-C covalent cross-linking of the overlapping graphene sheets in the aerogel, resulting in increase of the mechanical strength after annealing [25].

These unsaturated carbon sites provide an opportunity for the neighboring sp3 hybridized carbon atoms to undergo a transition to a more energetically favorable sp2 hybridization. This transition involves the reorganization of electron orbitals, resulting in the formation of planar hexagonal structures characteristic of graphene. The conversion of sp3 carbons to sp2 (see Figure 12) carbons contributes to the restoration of a more graphitic and ordered carbon lattice in the aerogel, this phenomenon is also called graphitization.

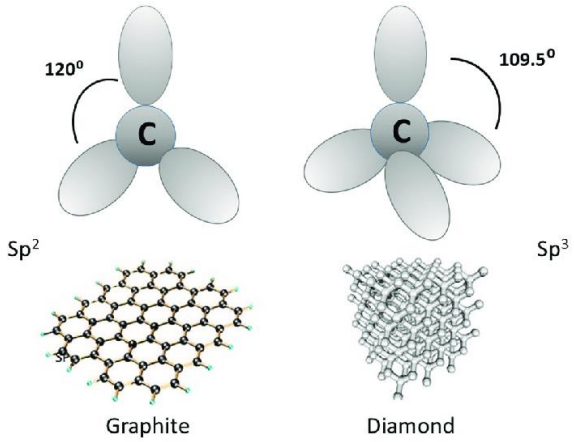

Figure 12: Illustration of sp2 and sp3 carbons [26].

This graphitization has major consequences on the GO aerogel. As the carbon atoms in the graphene sheets become more ordered and arranged in a more crystalline structure, it can lead to the restructuration of the aerogel and formation of well-defined pores as can be seen on Figure 6 between the pictures a and d; pictures c and f, where smoother surfaces and bigger pores are displayed after annealing. Thus, it increases in the overall surface area, contributing to enhanced pore volume.

Also, in her work Kabiri S. and al. (2014) displayed a super oleophilic GO aerogel with a contact angle of 0. They found that, after annealing, the GO aerogels present a higher selectivity towards the oils because of the high degree of p electron delocalization conjugated system on the surface of the graphene, due to the sp2 hybridization of the carbon atoms after hydrothermal and chemical reduction of GO. [27].

Moreover, since annealing involves heating the material to high temperatures, it helps in the removal of volatile components. In the case of graphene aerogels, this can include the removal of residual solvents, water, or other volatile substances that might be present after the aerogel fabrication process. The removal of these components can also contribute to an increase in pore volume.

One problem of the GO aerogels are the closed pores, which are inaccessible to fluids as displayed on Figure 13, hindering the effective interaction between the aerogel and the oil to be absorbed. These closed pores limit the aerogels' overall surface area available for sorption, leading to reduced oil sorption capacities and therefore the small number of oil occupied pores. Annealing can reduce them via the heating and cooling cycles that induce thermal expansion and contraction in the material. This dynamic process can help break apart and reshape the structure, potentially mitigating the formation of closed pores or reopening existing ones.

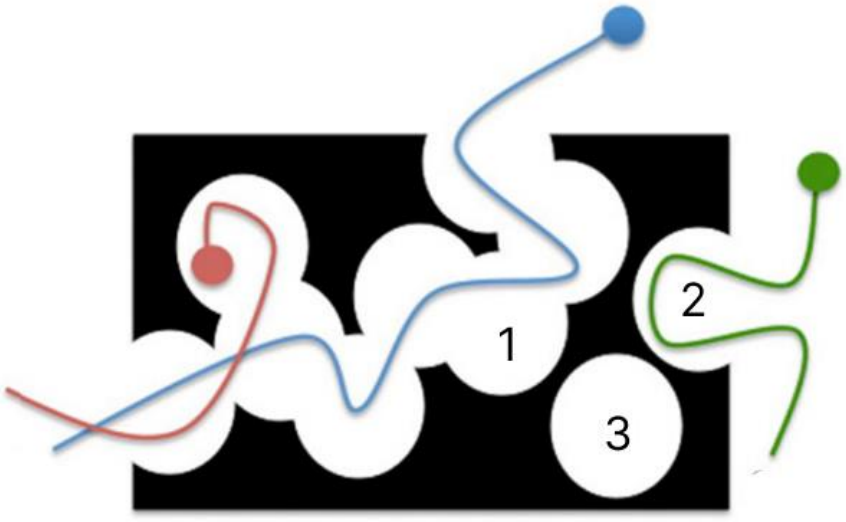

Figure 13: Illustration of open pores (1,2) and closed pores (3). [28]

Therefore, because of an higher hydrophobicity with the removal of the oxygen groups and volatile components at 800°C, better oil selectivity and higher pore volume due to the graphitization and removal of some closed pores due to thermal expansion, the annealed aerogels on Figure 10a and b display better pore volume, better oil filled pores and better sorption capacities than the ones who were not annealed.

B. Effect of freeze-casting

Freeze casting is a fabrication technique that involves the controlled solidification of a solution or suspension by freezing. During this process, ice crystals form a template within the material, which is subsequently removed by freeze-drying, having significant effects on the morphology and the properties of GO aerogels.

From the Figure 14a, the sorption capacity (respectively sorption rate) of freeze casting at -20°C compared to freeze casting at -200°C are as follows:

From 178,41 mg/mg (1,86 (mg/mg)/s) to 66,81 mg/mg (0,52 (mg/mg)/s) for canola oil, from 155,15 mg/mg (1,57 (mg/mg)/s) to 63,36 mg/mg (0,55 (mg/mg)/s) for olive oil and from 123,71 mg/mg (1,05 (mg/mg)/s) to 64,39 mg/mg (0,57 (mg/mg)/s) for motor oil.

Therefore, the curves show a clear trend of decreasing sorption capacity and sorption rate values with the decrease in temperature.

From the Figure 14b, the pore occupancy (respectively ratio to the total volume) of FC at -20°C compared to FC at -200°C are as follows:

From 0,120 cm^3/mg (68%) to 0,045 cm^3/mg (25%) for canola oil, from 0,138 cm^3/mg (78%) to 0,056 cm^3/mg (29%) for olive oil and from 0,138 cm^3/mg (71%) to 0,073 cm^3/mg (43%) for motor oil.

Therefore, the pore occupancy of the oil displays the same trend, decreasing with the decrease in temperature. Moreover, it is important to note that all the aerogels had similar, if not the same, total pores volume.

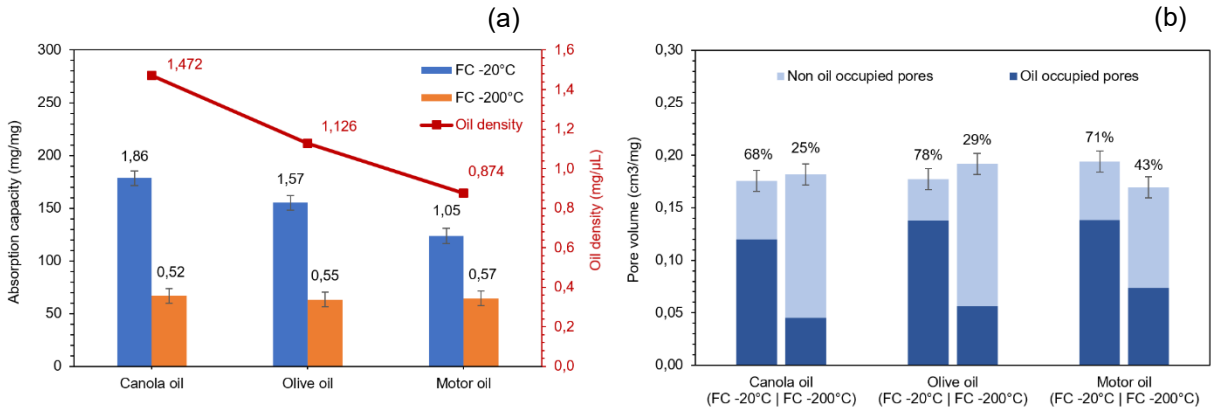

Figure 14: Study of the freeze casting method influence by comparison of sorption capacity and sorption rate ((mg/mg)/s, values indicated in the plot) between GO2VC2.5_TT and GO2VC2.5*_TT for different oils (a), comparison of the pore volume occupied by the oil (percentage of total volume indicated in the plot) between GO2VC2.5_TT and GO2VC2.5*_TT (b).

Those decreasing trend from -20°C to -200°C can be explained by the fact the morphology temperature of the freeze casting has an impact on the morphology network as seen earlier with the SEM pictures on Figure 6. By strategically adjusting freezing temperatures during the freeze casting process, we can effectively regulate the porosity of GO aerogels over a wide range.

In their work X. Xie and al. (2013) performed water absorption on cross-sections of GO aerogels for different positions [20]. Their results are displayed in Figure 15. It was found out that if the aerogel is being freeze-casted at temperatures around -200°C, it yields an isotropic structures throughout the whole material, with a cellular-like microstructure and small pores as could have been seen on Figure 6b. This isotropic structure is due to the nucleation of the ice crystals that is so fast, happening everywhere simultaneously that the newly formed germs do not have space to grow.

However, when being freeze-casted at temperature between -20°C and -50°C, the material tends to exhibit an anisotropic structure because of slow growth of the ice crystals along the temperature gradient. Therefore, this inhomogeneous freezing creates two distinct microstructures that can be observed, at the center and at the edges. At the center, distinguishable sheets without order can be observed as in Figure 6a. Meanwhile on the edges layered sheets with thinner borders can be seen.

X. Xie and al. (2013) found that the determining factor of water absorption of a graphene sponge is their mean pore size. They also showed that the aerogel freeze-casted at temperature at around -170°C displayed water absorbent properties because this temperature gradient yielded pores sizes inferior to 150 µm, meanwhile submitting aerogel to temperature superior to -20°C displayed water resistant properties because this temperature gradient yielded pores sizes superior to 300 µm. [20]. However, if frozen at temperatures between -20°C and -50°C, the aerogel displayed both of those properties, being water absorbent in the center and water resistant on the edge, forming like a water-resistant shell around the center, preventing the penetration of water.

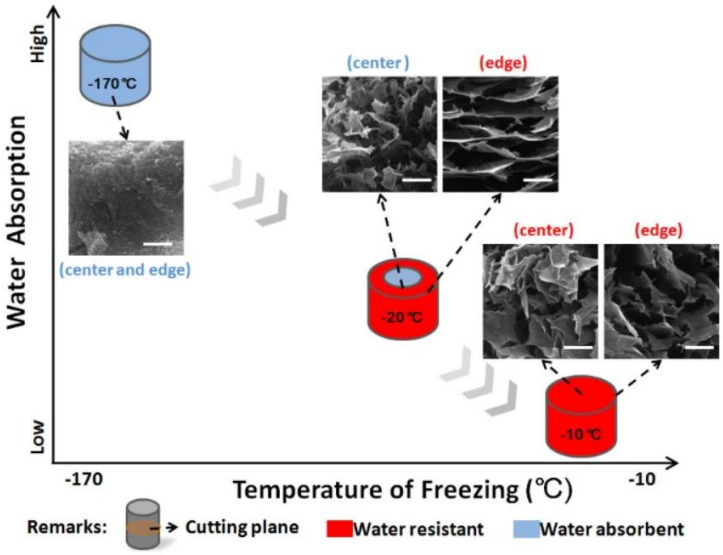

Figure 15: Water absorption and resistance aerogel properties with respect to freezing temperature of freeze casting. [20]

Therefore, when comparing the discoveries of X. Xie and al. (2013) with the paper sorption results, the difference between the results can be explained as follows, on one's hand, having a certain volume of closed pores, as discussed in effect of annealing, the aerogel prepared via the -200°C freeze casting is prone to water absorption to a certain amount during the deposition on the water bed in the beaker, meaning that less volume would be available for the oil during the sorption, involving a lower sorption capacity that have been demonstrated on Figure 14b with, for the canola oil, an pore occupancy of 68% for the freeze casting with conventional freezer compared to only 25% for the freeze casting with liquid nitrogen. On the other hand, the aerogel prepared with the -20°C freeze casting does also present a certain number of closed pores but is less susceptible to have water filled pores preventing the oil storage thanks to their water-resistant edges and thus absorbing more oil, implying better sorption capacity.

C. Effect of reducing agent

In the synthesis of GO aerogel through a hydrothermal approach, a reducing agent is crucial for the reduction of graphene oxide sheets, which are initially oxidized. Here, two reducing agents are considered: Vitamin C (VC) and ethylenediamine (EDA).

From the Figure 16a, the sorption capacity (respectively sorption rate) of VC compared to EDA are as follows:

From 178,41 mg/mg (1,86 (mg/mg)/s) to 405,24 mg/mg (3,62 (mg/mg)/s) between GO2VC2.5_TT and GO2EDA2.5_TT, from 165,88 mg/mg (1,50 (mg/mg)/s) to 191,45 mg/mg (1,60 (mg/mg)/s) between GOx1VC2.5_TT and GOx1EDA2.5_TT and from 39,62 mg/mg (0,33 (mg/mg)/s) to 169,23 mg/mg (1,22 (mg/mg)/s) between GOx1VC2.5 and GOx1EDA2.5.

Therefore, the curves show a clear trend of better sorption capacity and sorption rate values with the EDA compared to the VC.

From the Figure 16b, the pore occupancy (respectively ratio to the total volume) of VC to EDA are as follows:

From 0,120 cm^3/mg (68%) to 0,328 cm^3/mg (39%) between GO2VC2.5_TT and GO2EDA2.5_TT, from 0,111 cm^3/mg (56%) to 0,129 cm^3/mg (16%) between GOx1VC2.5_TT and GOx1EDA2.5_TT and from 0,027 cm^3/mg (12%) to 0,089 cm^3/mg (11%) between GOx1VC2.5 and GOx1EDA2.5.

Thus, the pore occupancy of canola oil displays the same trend, increasing with the EDA compared to the VC. Moreover, it is important to note that the aerogels reduced with EDA showed higher pore volume, as much as three times more, than compared to the VC reduced aerogels.

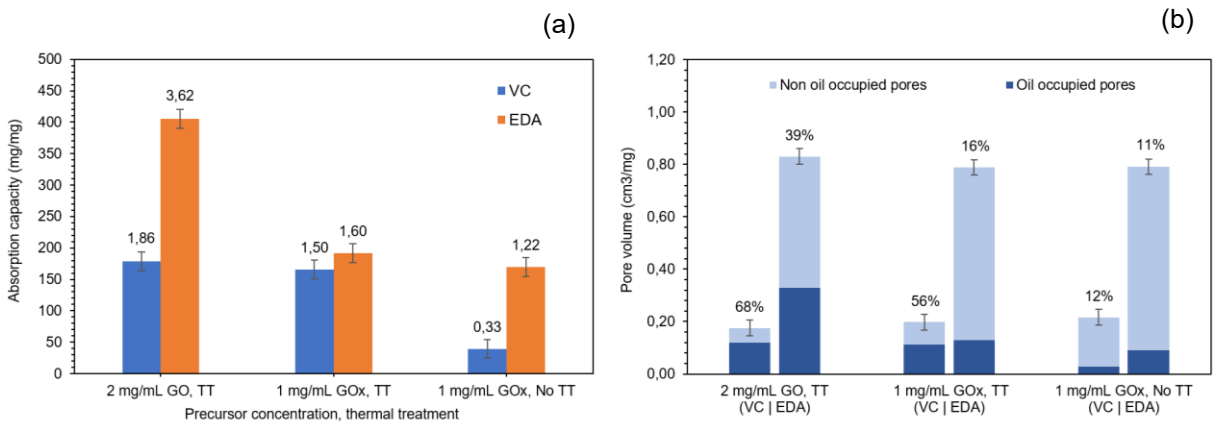

Figure 16: Study of the reducing agent influence by comparison of sorption capacity and sorption rate ((mg/mg)/s, values indicated in the plot) between GO2VC2.5_TT and GO2EDA2.5_TT, GOx1VC2.5_TT and GOx1EDA2.5_TT, GOx1VC2.5 and GOx1EDA2.5 for canola oil (a), comparison of the pore volume occupied by canola oil (percentage of total volume indicated in the plot) between GO2VC2.5_TT and GO2EDA2.5_TT, GOx1VC2.5_TT and GOx1EDA2.5_TT, GOx1VC2.5 and GOx1EDA2.5 (b).

The same way as presented earlier with annealing, the main goal of a reducing agent is to reduce the graphene oxide, to remove the numerous oxygen functions in order to enhance the hydrophobicity of the aerogel and to restore the graphene-like structure. The successive reducing steps and structure of aerogels are showed on Figure 17.

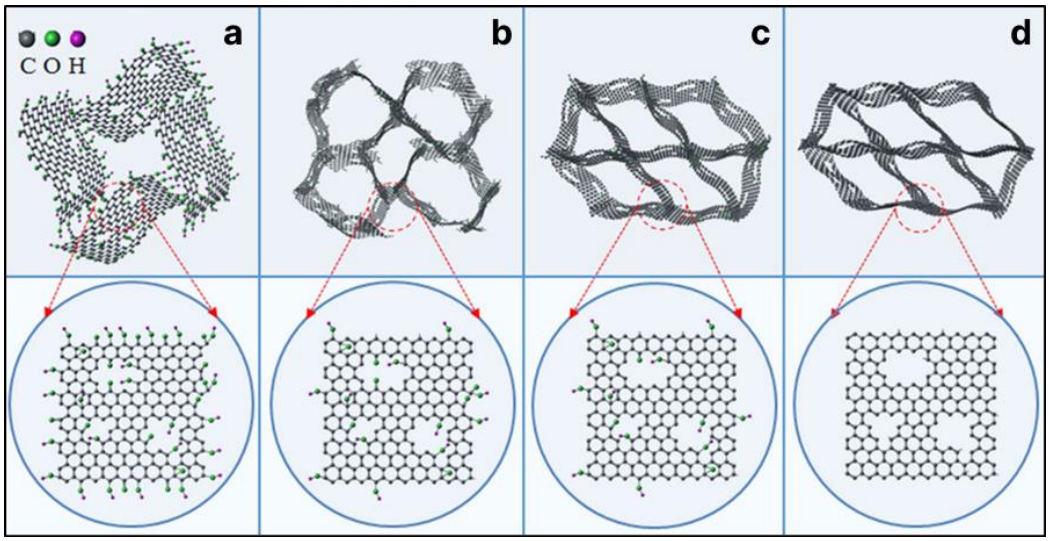

Figure 17: Illustration of the evolution of the functional groups on the lattice: GO aqueous dispersion (a), graphene hydrogel (b), dried graphene hydrogel or graphene aerogel (c) annealed graphene aerogel (d) [29].

Vitamin C, also known as ascorbic acid, has a better reducing capacity than ethylenediamine as a reducing agent. Is this mainly due to their functional groups, VC having multiple hydroxyl groups -OH and EDA having amino groups -NH.

Based on Wan W. and al. work (2016) [30], they marked multiples important points on the influence of the reducing agent on the sorption properties of GO aerogels. They showed that VC demonstrated the strongest reduction ability, leading to a higher reduction degree, meanwhile EDA demonstrated lower reduction ability and left hydrophilic groups such as N-H on the aerogel. For this reason, VC performed better hydrophobicity than EDA, showed by water angle tests. Moreover, because of its strong reduction effect, VC promotes crosslinking between the GO sheets, causing the 3D network becomes narrower and branched, leading to smaller pore sizes. [31]

They also revealed that the pH of the solution containing the reducing agent played an important role on the pores size. The vitamin C solution displayed a pH of 3,4 (acidic solution) and the EDA solution displayed a pH of 10,4 (alkaline solution). However, alkaline solutions yield graphene sheets with large size and thus large pores, meanwhile acidic solutions yield agglomerated graphene sheets, as can been seen on Figure 6a, and thus smaller pores [30].

For those reasons EDA reduced aerogels showed in Figure 16b bigger pores volume than the VC reduced aerogels, however VC reduced aerogels showed a bigger oil occupied volume ratio to the total volume because of their enhanced hydrophobicity and thus better selectivity to the oils. EDA reduced aerogel showed better sorption capacities only because of their larger pores volume (more than twice the volume of VC reduced aerogel), despite their lower hydrophobicity.

D. Effect of precursor concentration

The precursor concentration plays a crucial role in the synthesis of graphene oxide aerogels, influencing their structural, morphological, and sorption properties. In the context of graphene aerogel fabrication, a precursor refers to the initial substance or solution from which the graphene oxide structure is derived. In this part, the precursor analysed is expended graphene oxide (GOx).

From the Figure 18a, the sorption capacity (respectively sorption rate) of GOx precursor concentration of 0,5 mg/mL compared to GOx precursor concentration of 1 mg/mL are as follows:

From 193,57 mg/mg (1,44 (mg/mg)/s) to 165,88 mg/mg (1,50 (mg/mg)/s) for canola oil, from 160,87 mg/mg (1,40 (mg/mg)/s) to 133,42 mg/mg (1,10 (mg/mg)/s) for olive oil and from 124,40 mg/mg (0,97 (mg/mg)/s) to 114,95 mg/mg (0,98 (mg/mg)/s) for motor oil.

Therefore, the curves show a clear trend of decreasing sorption capacity values with the increase of precursor concentration, the sorption rate remains more or less the same with either precursor concentration.

From the Figure 18b, the pore occupancy (respectively ratio to the total volume) of GOx precursor concentration of 0,5 mg/mL compared to of 1 mg/mL are as follows:

From 0,130 cm^3/mg (32%) to 0,111 cm^3/mg (56%) for canola oil, from 0,143 cm^3/mg (34%) to 0,119 cm^3/mg (62%) for olive oil and from 0,139 cm^3/mg (33%) to 0,128 cm^3/mg (70%) for motor oil.

Therefore, the pore occupancy of the oil displays the same trend, increasing slightly with the decrease of precursor concentration. Moreover, it is important to note that all the aerogels had similar, if not the same, oil occupied pores even if the aerogels with a lower precursor concentration have better pore volume than the ones with bigger precursor concentration.

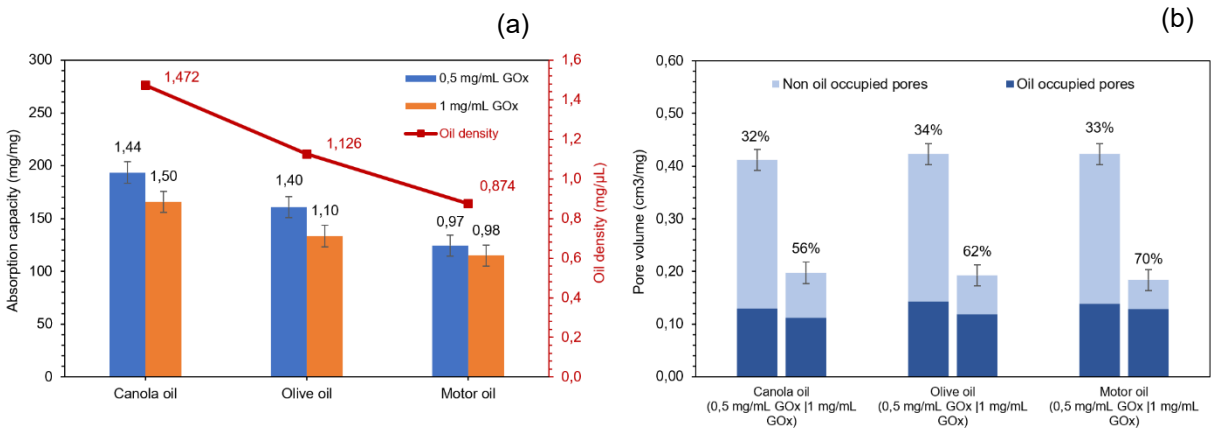

Figure 18: Study of the material concentration influence by comparison of sorption capacity and sorption rate ((mg/mg)/s, values indicated in the plot) between GOx0.5VC2.5_TT and GOx1VC2.5_TT for different oils (a), comparison of the pore volume occupied by the oil (percentage of total volume indicated in the plot) between GOx0.5VC2.5_TT and GOx1VC2.5_TT (b).

From the Figure 19a, the same trend on the decreasing sorption capacity values with the increase of precursor concentration can be observed, similarly to Figure 18a. The sorption capacity (respectively sorption rate) of GOx precursor concentration of 0.5 mg/mL compared to GOx precursor concentration of 1 mg/mL are as follows:

From 85,32 mg/mg (0,67 (mg/mg)/s) to 39,62 mg/mg (0,33 (mg/mg)/s) between GOx0.5VC2.5 and GOx1VC2.5, from 193,57 mg/mg (1,44 (mg/mg)/s) to 165,88 mg/mg (1,50 (mg/mg)/s) between GOx0.5VC2.5_TT and GOx1VC2.5_TT.

From the Figure 19b the pore occupancy of the oil displays also the same trend as in Figure 18b, decreasing slightly with the increase of precursor concentration. The pore occupancy of GOx precursor concentration of 0,5 mg/mL compared to 1 mg/mL are as follows:

From 0,057 cm^3/mg (16%) to 0,027 cm^3/mg (12%) between GOx0.5VC2.5 and GOx1VC2.5, from 0,130 cm^3/mg (32%) to 0,122 cm^3/mg (56%) between GOx0.5VC2.5_TT and GOx1VC2.5_TT.

Moreover, it is also important to note that the aerogels with a lower precursor concentration have better pore volume than the ones with bigger precursor concentration.

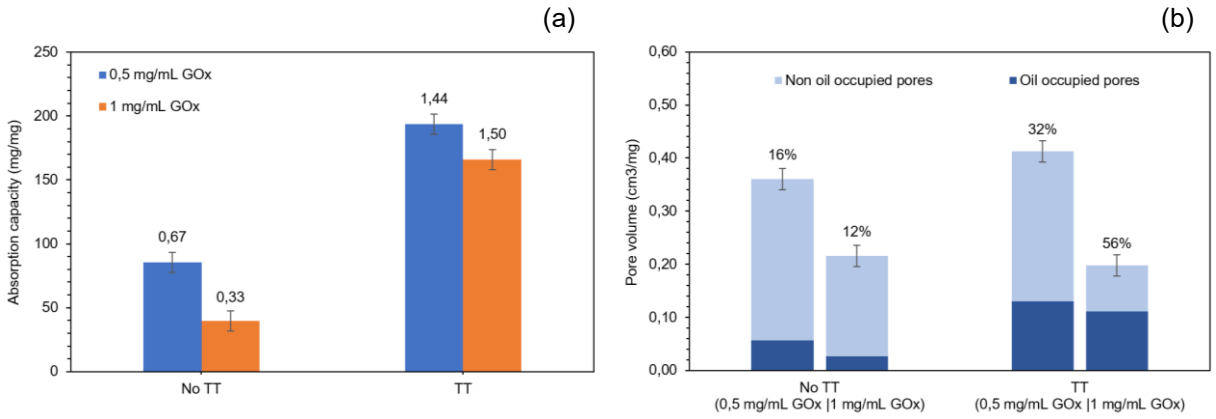

Figure 19: Study of the material concentration influence by comparison of sorption capacity and sorption rate ((mg/mg)/s, values indicated in the plot) between GOx0.5VC2.5 and GOx1VC2.5, GOx0.5VC2.5_TT and GOx1VC2.5_TT, for canola oil (a), comparison of the pore volume occupied by canola oil (percentage of total volume indicated in the plot) between GOx0.5VC2.5 and GOx1VC2.5, GOx0.5VC2.5_TT and GOx1VC2.5_TT (b).

From the literature, at lower precursor concentrations, the aerogels have smaller thinner wall and bigger pores, promoting more porous structures, as seen on Figure 20; but the mechanical strength is compromised, resulting in reduced stability and an increased susceptibility to shrinkage during heat treatment. This phenomenon of shrinkage not only diminishes the overall mechanical strength but also contributes to a decrease in pore volume. The lack of mechanical support at low concentrations allows for the sheets of graphene oxide to collapse and stack more closely, leading to a denser structure with limited porosity.

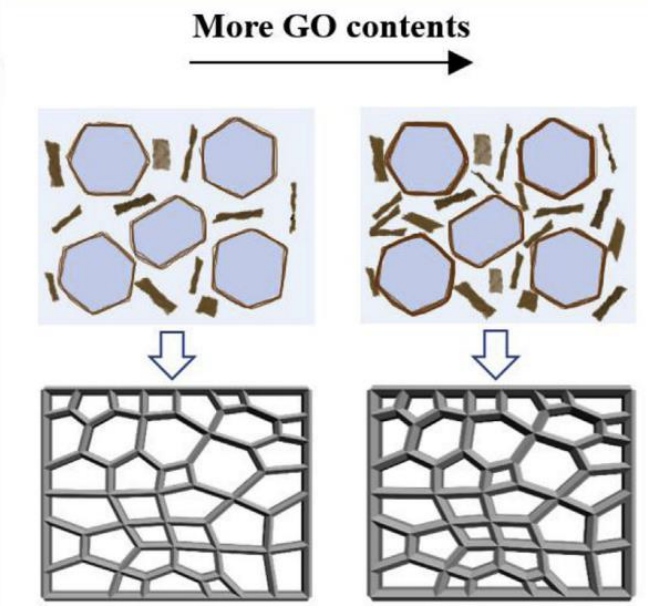

Figure 20: Effect of the precursor concentration on the wall thickness and pore volume [22].

Conversely, higher precursor concentrations improve the development of denser and more interconnected structures. The abundance of graphene oxide sheets in the solution increases the wall thickness and reduces the pores sizes but also increase the likelihood of crosslinking, resulting in a tighter network within the aerogel matrix. This interconnected network increases the mechanical strength but reduces the pore volume [32], [33], [34].

Therefore, optimal precursor concentrations strike a balance between preventing shrinkage of GO aerogel and preventing crosslinking and walls too thick.

Moreover, higher precursor concentrations play a role in limiting the growth of ice crystals during freeze casting. The increased presence of precursor occupies more space in the solution, impeding on the growth of ice crystals and consequently yielding smaller pores in the final aerogel structure of freeze casting [35].

Based on the findings depicted in Figure 18 and Figure 19, it is evident that a GOx concentration of 0,5 mg/mL yielded superior pore volume, as explained earlier. This concentration proves to be more optimal, enough to prevent aerogel shrinkage and thereby resulting in a bigger pore volume compared to a 1 mg/mL GOx concentration GO aerogel with denser crosslinking, thicker walls, and inhibited ice growth during freeze casting.

E. Influence of sorption process temperature

From the Figure 21a, the sorption capacity (respectively sorption rate) of the process temperature conducted at 24°C compared to 60°C are as follows:

From 165,88 mg/mg (1,50 (mg/mg)/s) to 191,13 mg/mg (1,82 (mg/mg)/s) for GOx1VC2.5_TT; from 191,45 mg/mg (1,60 (mg/mg)/s) to 362,44 mg/mg (3,65 (mg/mg)/s) for GOx1EDA2.5_TT.

Therefore, the curves show a trend of increasing sorption capacity and sorption rate values with the increase of the sorption process temperature.

From the Figure 21b, the increasing pore occupancy of the process temperature conducted at 24°C to 60°C are as follows:

From 0,111 cm^3/mg (56%) to 0,168 cm^3/mg (61%) for GOx1VC2.5_TT and from 0,129 cm^3/mg (16%) to 0,319 cm^3/mg (29%) for GOx1EDA2.5_TT.

Therefore, the pore occupancy of canola oil displays the same trend, increasing with the sorption process temperature.

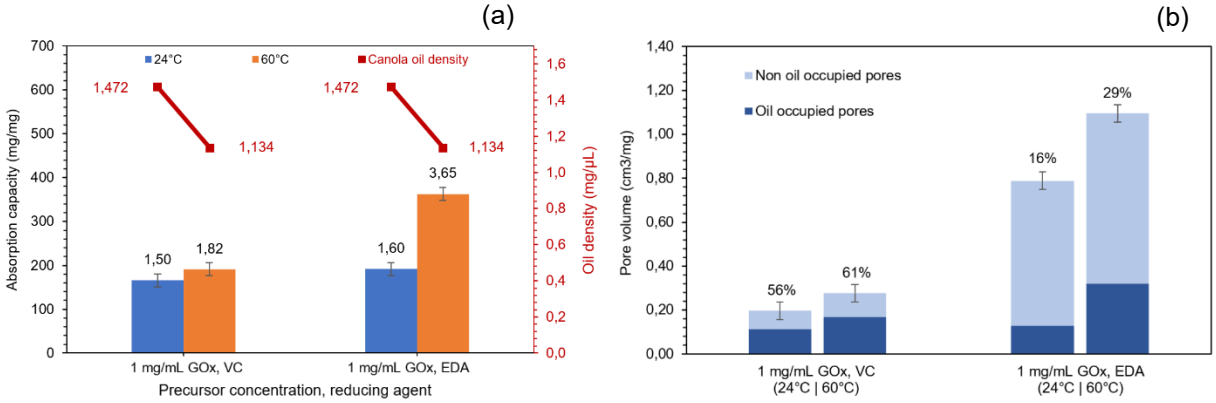

Figure 21: Study of the sorption process temperature influence by comparison of sorption capacity and sorption rate ((mg/mg)/s, values indicated in the plot) for GOx1VC2.5_TT at 24°C and 60°C and GOx1EDA2.5_TT at 24°C and 60°C for canola oil (a), comparison of the pore volume occupied by canola oil (percentage of total volume indicated in the plot) between for GOx1VC2.5_TT at 24°C and 60°C and GOx1EDA2.5_TT at 24°C and 60°C (b).

Adjusting the temperature during the oil sorption process significantly influences the performance of GO aerogels as seen above. The higher temperatures not only boost the sorption capacity by enhancing the kinetic energy of oil molecules but also play a role in enhancing the wettability of the aerogel surface. This improvement in wetting and penetration is attributed to the temperature-induced changes in the viscosity and surface tension of the oil [36]. As an example, the viscosity of canola oil goes from 46,2 cP at 30°C to 17,21 cP at 65°C [37], [38] demonstrating the loss of viscosity and thus enhancement of the fluidity, penetrating better in the pores, thus yielding better oil occupied pores and improving the sorption capacity.

Moreover, the kinetics of the sorption process are notably affected by temperature, with elevated temperatures accelerating molecular movement and increasing the rate of oil uptake by the aerogel. Thus, the faster sorption rate on Figure 21a This higher thermal energy facilitates a faster diffusion of oil molecules into the aerogel structure.

It is for the same reason that all along the tests performed earlier, canola oil was better absorbed inside the aerogels and showed better sorption rate at 24°C (71,7 cP [38]) compared to olive oil (84 cP [39]) and then motor oil (206,89 cP [40]).

Additionally, the structural changes induced by elevated temperatures are essential to consider. While higher temperatures can bring modifications in the porosity, surface area, and surface chemistry of some materials, it's important to note that GO aerogels exhibit minimal structural changes in response to temperature variations due to their small thermal expansion coefficient of 10^{-6} K^{-1} [41].

3. Density measurements

The sorption capacity of GO aerogels exhibits an important correlation with the density of adsorbed oils, as observed in various studies [14], [27], [42], [43]. From the sorption experiments, the data reveal that the adsorption capacity increases with the density of oil and a linear relationship between the weight gain of GO aerogels and the density of organic solvents can be highlighted, as seen on Figure 22.

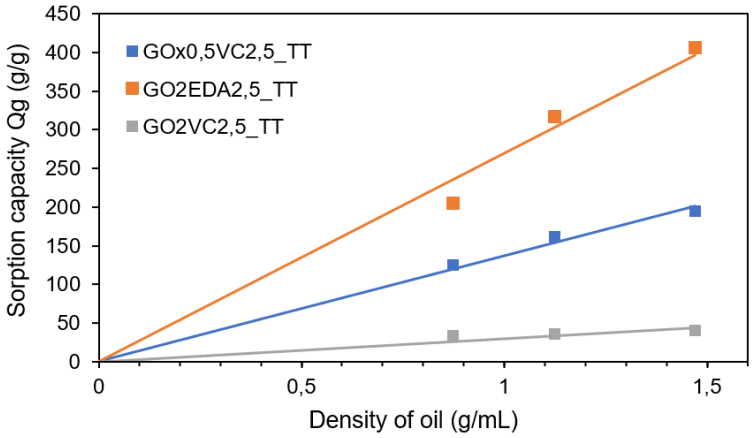

Figure 22: Linear relationship between the oil density and the sorption capacity for different GO aerogels.

Therefore, from those data of canola, olive and motor oil, this linear relationship can be described as follows:

$$Q_g\,(mg/mg) = k * \rho_{organic} \quad (6)$$

Where Q_g is the aerogel sorption capacity in mg/mg, k is the slope of the linear equation, in µL/mg and $\rho_{organic}$ is the density of the organic liquid, in mg/µL. From the units m is representative of the oil volume occupied per unit mass of graphene oxide aerogel.

The importance of this formula relies on its predictive understanding, as the linear correlation provides a predictive model for estimating the sorption capacity based on the density of the oil. Thus, by incorporating this formula, it becomes a valuable tool for assessing and predicting the overall performance of a GO aerogel in oil sorption scenarios.

The performance of the tested aerogels is listed in Table 2. Based on the slope k of the linear equation, the best performing aerogels are as follows: GO2EDA2.5_TT, GOx1EDA2.5_TT, GOx0.5VC2.5_TT, GOx1EDA2.5, GO2VC2.5_TT, GOx1VC2.5_TT, GOx0.5VC2.5, GO2VC2.5*_TT and GOx1VC2.5.

This is in line with the results shown earlier, as the best performing aerogel are EDA reduced, post treated with annealing, freeze-casted at -20°C and with the lower precursor concentration.

Aerogel	k (µL/mg)	R^2
GO2VC2.5_TT	129,91	0,9951
GO2VC2.5*_TT	53,82	0,9633
GOx1VC2.5	30,12	0,9821
GOx1VC2.5_TT	117,87	0,9966
GOx0.5VC2.5	54,58	0,9959
GOx0.5VC2.5_TT	136,90	0,9985
GO2EDA2.5_TT	269,56	0,996
GOx1EDA2.5	135,16	0,9618
GOx1EDA2.5_TT	143,77	0,9902

Table 2: Performance of oil sorption of the tested aerogels.

4. Discussion and comparison with literature

To compare the sorption capacity with those of the literature [2], two aerogels were chosen, GO2EDA2.5_TT, which showed the best sorption capacity and GO1VC2.5_TT, which showed the less dislocation and thus, which is the most promising in terms of reusability. The values are displayed in Table 3.

Material type	Oil type	Sorption capacity (g/g)	Reusability (reported by authors)	Ref.
Cellulose fiber	Heavy crude oil	5	_	[6]
Polypropylene	Light crude oil	10	Yes	[7]
Organoclay	Engine oil	2,1 - 3,6	No	[44]
Raw cotton	Crude oil	30 - 40	Yes	[7]
Cotton lint	Crude oil	80	Yes	[45]
Silkworm cocoon	Motor oil	42 - 52	Yes	[8]
CF3 functionalized silica aerogel	Crude oil	237	Yes	[46]
Exfoliated graphite	Heavy crude oil	86	Yes	[6]
Graphene aerogel	Diesel oil	105,93	_	[14]
GO1VC2.5_TT (Graphene aerogel)	Canola oil + dye	165,88	Not tested	This paper
GO2EDA2.5_TT (graphene aerogel)	Canola oil + dye	405,24	No	This paper

Table 3: Comparison of materials used in oil sorption.

From the compared results in Table 3, we can observe that among all the materials, the graphene aerogel synthesized in this paper (GO2EDA2.5_TT) showed the best sorption capacity, followed by a CF3 functionalized silica aerogel and by another aerogel synthesized in this paper (GO1VC2.5_TT).

However, those good sorption capacities are mitigated by the non-reusability of the aerogel after sorption of the oils and the poor oil volume occupancy displayed for the EDA reduced aerogel.

The limited oil pore occupancy in GO aerogels during oil sorption experiments is due to a combination of factors with distinct impacts on sorption performance.

The freeze casting process plays a crucial role on this limited pore occupancy by creating a water-resistant phase at the edges and a water-absorbent phase at the center of the aerogel. The cut location before testing is essential, as a mid-section cut may overestimate water absorption and decrease the number oil filled pores, while an edge cut improves sorption capacity by excluding the water-resistant phase, preventing water penetration into the pores. Therefore, comparing a center cut aerogel and edge cut aerogel can lead to non-representative results.

In the case of EDA reduced aerogels, despite exhibiting superior oil sorption performance compared to VC reduced aerogels, it displays less hydrophobicity. Thus, prolonged exposure to atmospheric conditions or on waterbed during the experiment can permit water infiltration into the pores, restricting available space for oil sorption. To optimize the oil sorption, good conservation practices are essential to mitigate undesired water penetration.

Mechanically, EDA-reduced aerogel also confronts issues related to its structural integrity. Despite its enhanced oil sorption, the aerogel's large pores, supported by smaller walls, are susceptible to collapse, particularly when exposed to dense oils with high viscosity.

Dense oils, especially those with elevated viscosity such as motor oil in this paper, possess considerable mass and resistance to flow. Upon entering the aerogel pores, these oils exert forces on the surrounding graphene sheets that constitute the backbone of the aerogel. Under the pressure of the oil, graphene sheets may undergo deformation or stacking, reducing the available pore volume for oil sorption, and damaging the overall stability of the aerogel.

Depending on the elasticity of the aerogel, it may exhibit limited ability to recover its original structure after deformation caused by the forces exerted by the oil. If the aerogel lacks sufficient elasticity or if the forces are too intense, irreversible structural changes may occur such as the dislocation of the aerogel shown in Figure 23. the collapse of the aerogel's porous structure, hindering the maintenance of an open porous network.

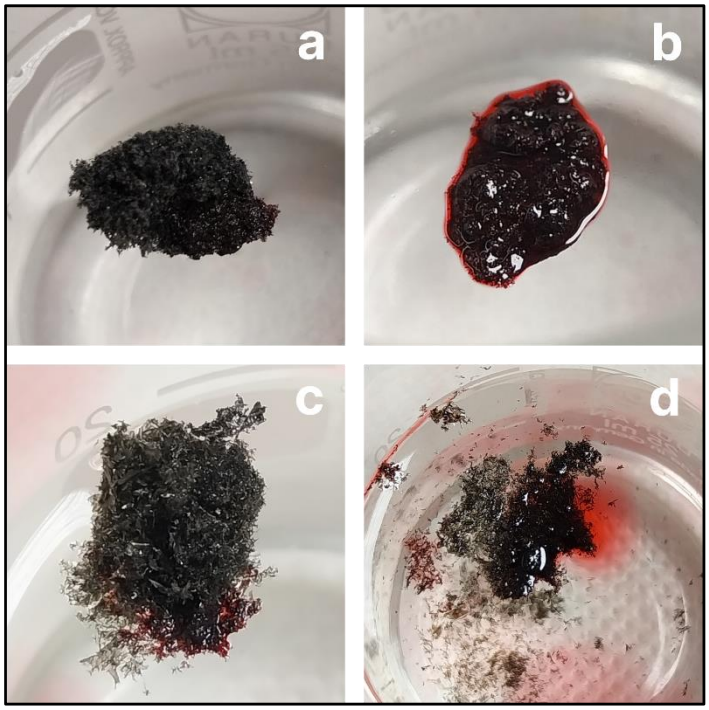

Figure 23: Pictures of GO aerogel, VC reduced before sorption test (a), after sorption test (b), EDA reduced before sorption test (c), after sorption test (d).

Moreover, when EDA-reduced aerogel is at lower precursor concentrations, the mechanical strength is further compromised as smaller and thinner walls at lower concentrations create larger pores, promoting a more porous structure that is inherently less resistant to external forces, resulting in reduced stability and increased susceptibility collapse under the forces exerted by the penetration of dense and viscous oils.

The consequence of this mechanical instability manifests in the disintegration of the aerogel post-sorption, particularly pronounced in EDA reduced aerogels. This disintegration hinders recycling, as the sample is destroyed, and compression release becomes impossible for physically removing the oil.

Consequently, the observed oil-filled pores can sometime constitute only a fraction of the total pore volume in the aerogel, underscoring the need for a delicate balance between oil sorption efficiency and structural integrity.

IV. Conclusion

In this thesis, sorption tests of different graphene oxide aerogels were reported and showed the effects of several parameters on sorption properties.

In first place, the use of freeze casting with a temperature of - 20°C has shown better results than with a temperature of -200°C due to the enhanced hydrophobicity thanks to the creation of a water-resistant layer, and improved pore volume. However, depending on the processing of the -20°C freeze-casted aerogel, an only water absorbent phase can be selected, decreasing the sorption performance.

In the same way, post treated aerogel with annealing, showed better sorption performance, mainly due to the graphitization of the aerogel's structure and removal of volatile components.

The increase of the sorption process temperature led to better sorption capacities and sorption rates because of the temperature-induced changes in the viscosity and surface tension of the oil, penetrating easier and faster the pores of the aerogel.

On the precursor concentration, lower concentrations yield aerogels with more porous structures, characterized by smaller walls and larger pores, however at the expense of mechanical strength and stability. While higher concentrations result in denser, interconnected structures, improving mechanical strength but reducing pore volume. Striking the optimal balance is crucial to prevent shrinkage and excessive crosslinking and thus obtaining the best performances.

Depending on use, the reducing agent of GO aerogel can be modified to correspond to the requirement.

For an oil spill catastrophe that happen rarely but have a big volume of oil spilled, an aerogel with fast sorption rate and big sorption capacity aerogel will be preferred. In that case, an aerogel synthetized with EDA reducing agent is considered as the best option even without recycling, as the emphasis is given on the prevention of the oil not reaching the shore and harming the wildlife then having an interesting economic cost. In this thesis, following the synthesis parameter mentioned above, an aerogel with 405,24 mg/mg with 3,62 (mg/mg)/s oil sorption rate for canola oil has been synthesized.

For a domestic kitchen oil spill or oil pump spill, the effects are less dangerous and doesn't need immediate intervention as for an oil spill catastrophe but have a bigger emphasis on the recycling capacity, in that case, an aerogel synthetized with, VC reducing agent is considered as the best option. In this thesis, following the synthesis parameter mentioned above, an aerogel with 193,57 mg/mg with 1,44 (mg/mg)/s sorption rate for canola oil has been synthesized.

For future work, it may be interesting to investigate the sorption properties of GO aerogels by varying their reducing agent w/w ratio, varying the annealing parameters and to investigate on their mechanical properties for reuse via compression or burning.

V. Budget

Planning and monitoring a project's budget are one of the most important parts to ensure its viability. Therefore, in this section, an overall estimation of this thesis cost will be discussed through cost tables.

In the first place, the details of the project director's supervision, the utilization of the SEM by the laboratory technician, and the engineering student's work on manipulation and experimentation in the university laboratory are presented in Table 4.

Type of labor	Cost per hour (€/h)	Number of hours (h)	Cost (€)
Project director/Tutor	25	50	1250
Laboratory technician	17	2	34
Engineer student	15	250	3750
Total			**5034**

Table 4: Labor cost of the work.

Next, the use of the machinery equipment is taken into account. The cost per hour of machinery is mainly based on its energy consumption and its depreciation. The estimated costs are displayed in Table 5.

Machinery equipement	Cost per hour (€/h)	Number of hours (h)	Cost (€)
SEM	30	2	60
Ultra-sonic bath	0,4	11	4,4
Freezer	1	528	528
Oven	2	6	12
Hot plate	1	8	8
Precision balance	1	4	4
Total			**616,4**

Table 5: Machinery equipment use cost of the work.

Lastly, the expenses associated with the materials and tools utilized are calculated, with detailed estimations available in Table 6 below. However, it is crucial to highlight that some tools can be reused and could be employed again on another project. Hence, the budget for this section is intentionally set with an overestimation.

Material and tool	Cost (€/quantity)	Quantity	Cost (€)
GO	100€/200mg	110 mg	55
VC	15€/250g	15 mg	0,0009
EDA	42,70€/707g	10 mg	0,0006
Motor oil 5W-40	8,50€/L	3 mL	0,255
Canola oil	3,50€/L	3 mL	0,0105
Olive oil	12,50€/L	3 mL	0,0375
Dye	12€/L	1 mL	0,012
Liquid nitrogen	2€/L	2 L	4
Distilled water	8€/5L	1,125 L	1,8
Acetone	15 €/L	0,01 L	0,15
Becker	11€/unit	4 units	44
Micropipette	366€/unit	1 unit	366
Tweezers	7,50€/unit	1 unit	7,5
Tape	3,50€/unit	0,05 unit	0,175
Petri dishes	30€/unit	3 units	90
Scissors	2,30€/unit	1 unit	2,3
Scalpel	168€/100units	1 unit	1,68
Caliper	16€/unit	1 unit	16
Spatula	4,50€/unit	1 unit	4,5
Stopwatch	7€/unit	1 unit	7
Graduated cylinder	20€/unit	1 unit	20
Total			**620,4215**

Table 6: Materials and tools cost of the work.

In the end, by adding all the different costs, the total theorical cost of this thesis is 6270,83 € as shown in Table 7, knowing that this sum is the highest estimation. As said before, by reusing some tools of the lab, it could be, in reality, less expensive.

Category	Cost (€)
Labor	5034
Use of machinery equipement	616,4
Materials and tools	620,4215
Total	**6270,8215**

Table 7: Sum of the costs of the work.

References

[1] Anisuddin, S., Hashar, N. A., & Tahseen, S. (2005). Prevention of oil spill pollution in seawater using locally available materials. ResearchGate. https://www.researchgate.net/publication/242463950_Prevention_of_oil_spill_pollution_in_seawater_using_locally_available_materials

[2] Al-Majed, A., Adebayo, A. R., & Hossain, M. K. (2012). A sustainable approach to controlling oil spills. Journal of Environmental Management, 113, 213-227. https://doi.org/10.1016/j.jenvman.2012.07.034

[3] El-Ashtoukhy, E. Z., El-Taweel, Y., Abdelwahab, O., & Nassef, E. (2013). Treatment of petrochemical wastewater containing phenolic compounds by electrocoagulation using a fixed bed electrochemical reactor. International Journal of Electrochemical Science, 8(1), 1534-1550. https://doi.org/10.1016/s1452-3981(23)14117-4

[4] Duong, P. H., Chung, T., Wei, S., & Irish, L. (2014). Highly permeable Double-Skinned forward osmosis membranes for Anti-Fouling in the emulsified Oil–Water separation process. Environmental Science & Technology, 48(8), 4537-4545. https://doi.org/10.1021/es405644u

[5] Jamaly, S., Giwa, A., & Hasan, S. W. (2015). Recent improvements in oily wastewater treatment : progress, challenges, and future opportunities. Journal of Environmental Sciences, 37, 15-30. https://doi.org/10.1016/j.jes.2015.04.011

[6] Namita, T., Verma, V.K., Rai, J.P.N., 2006. Comparative evaluation of natural adsorbent for pollutants removal from distillery spent wash. J. Sci. Ind. Res. 65, 935e938.

[7] Choi, H.M., 1996. Needle punched cotton nonwovens and other natural fibers as oil cleanup sorbents. J. Environ. Sci. Health 31, 1441e1457

[8] Moriwaki, H., Kitajima, S., Kurashima, M., Hagiwara, A., Haraguchi, K., Shirai, K., Kanekatsu, R., Kiguchi, K., 2009. Utilization of silkworm cocoonwaste as a sorbent for the removal of oil from water. J. Hazard. Mater. 165 (1e3), 266e270.

[9] Fan ZJ, Yan J, Ning GQ, Wei T, Qian WZ, Zhang SJ, Zheng C, Zhang Q, Wei F (2010) Oil sorption and recovery by using vertically aligned carbon nanotubes. Carbon 48:4197–4200

[10] Tan, L., Yu, C., Wang, M., Zhang, S., Sun, J., Dong, S., & Sun, J. (2019). Synergistic effect of adsorption and photocatalysis of 3D G-C3N4-AGAR hybrid aerogels. Applied Surface Science, 467-468, 286-292. https://doi.org/10.1016/j.apsusc.2018.10.067

[11] Yan, S., Zhang, G., Li, F., Zhang, L., Wang, S., Zhao, H., Ge, Q., & Li, H. (2019). Large-area superelastic graphene aerogels based on a room-temperature reduction self-assembly strategy for sensing and particulate matter (PM2.5 and PM10) capture. Nanoscale, 11(21), 10372-10380. https://doi.org/10.1039/c9nr02071c

[12] Zhang, X., Zhang, T., Wang, Z., Ren, Z., Yan, S., Duan, Y., & Zhang, J. (2018). Ultralight, Superelastic, and Fatigue-Resistant Graphene Aerogel templated by graphene oxide liquid crystal stabilized air bubbles. ACS Applied Materials & Interfaces, 11(1), 1303-1310.

[13] Prună, A., Cárcel, A. C., Barjola, A., Benedito, A., & Giménez, E. (2019). Tailoring the performance of graphene aerogels for Oil/Organic solvent separation by 1-Step Solvothermal approach. Nanomaterials, 9(8), 1077. https://doi.org/10.3390/nano9081077

[14] Diao, S., Liu, H., Chen, S., Xu, W., & Yu, A. (2019). Oil adsorption performance of graphene aerogels. Journal of Materials Science, 55(11), 4578-4591. https://doi.org/10.1007/s10853-019-04292-z

[15] Bo, Y., Yu, A., Liu, H., Chen, S., Xu, W., Diao, S., & Zhang, C. (2020). Preparation of elastic graphene aerogel and its adsorption of oil. Journal of Porous Materials, 28(1), 39-56. https://doi.org/10.1007/s10934-020-00964-3

[16] https://www.nist.gov/laboratories/tools-instruments/nanofab-tool-zeiss-gemini-500-field-emission-scanning-electron

[17] Mohammed A., Abdullah A. Scanning electron microscopy (SEM): A review. Proceedings of 2018 International Conference on Hydraulics and Pneumatics – HERVEX. Romania. ISSN 1454 – 8003

[18] nanoscience Instruments. Components in a SEM. https://www.nanoscience.com/techniques/scanning-electron-microscopy/components/

[19] Akhtar F., Lecture – OM, SEM. T7003T. Division of Materials Science, Luleå University of Technology

[20] Xie, X., Zhou, Y., Bi, H., Yin, K., Wan, S., & Sun, L. (2013). Large-range control of the microstructures and properties of three-dimensional porous graphene. Scientific reports, 3(1), 1-6. https://doi.org/10.1038/srep02117

[21] Jung, S. M., Mafra, D. L., Lin, C., Jung, H. Y., & Kong, J. (2015). Controlled porous structures of graphene aerogels and their effect on supercapacitor performance. Nanoscale, 7(10), 4386-4393. https://doi.org/10.1039/c4nr07564a

[22] Liu, X., Pang, K., Yang, H., & Guo, X. (2020). Intrinsically microstructured graphene Aerogel exhibiting excellent mechanical performance and super-high

adsorption capacity. Carbon, 161, 146-152. https://doi.org/10.1016/j.carbon.2020.01.065

[23] Ren, Y., Zhou, T., Su, G., & Ma, Y. (2018). Online tracking of the thermal reduction of graphene oxide by two-dimensional correlation infrared spectroscopy. Vibrational Spectroscopy, 96, 32-45. https://doi.org/10.1016/j.vibspec.2018.02.010

[24] Kumar, P., Šilhavík, M., Zafar, Z. A., & Červenka, J. (2023). Universal strategy for reversing aging and defects in graphene oxide for highly conductive graphene aerogels. The Journal of Physical Chemistry C, 127(22), 10599-10608. https://doi.org/10.1021/acs.jpcc.3c01534

[25] Šilhavík, M., Kumar, P., Zafar, Z. A., Míšek, M., Čičala, M., Piliarik, M., & Červenka, J. (2022). Anomalous elasticity and damping in covalently cross-linked graphene aerogels. Communications Physics, 5(1). https://doi.org/10.1038/s42005-022-00806-5

[26] Theodosiou, A., Spencer, B. F., Counsell, J., & Jones, A. (2020). An XPS/UPS study of the surface/near-surface bonding in nuclear grade graphites : A comparison of monatomic and cluster depth-profiling techniques. Applied Surface Science, 508, 144764. https://doi.org/10.1016/j.apsusc.2019.144764

[27] Kabiri, S., Tran, D., Altalhi, T., & Lošić, D. (2014). Outstanding adsorption performance of graphene–carbon nanotube aerogels for continuous oil removal. Carbon, 80, 523-533. https://doi.org/10.1016/j.carbon.2014.08.092

[28] Patalano, A., Villalobos, F., Peña, P., Jauregui, E., Ozkan, C. S., & Ozkan, M. (2019). Scaling sorbent materials for real oil-sorbing applications and environmental disasters. MRS Energy & Sustainability, 6(1). https://doi.org/10.1557/mre.2019.3

[29] Cheng, Y., Zhou, S., Hu, P., Zhao, G., Li, Y., Zhang, X., & Han, W. (2017). Enhanced mechanical, thermal, and electric properties of graphene aerogels via supercritical ethanol drying and high-temperature thermal reduction. Scientific Reports, 7(1). https://doi.org/10.1038/s41598-017-01601-x

[30] Wan, W., Zhang, F., Yu, S., Zhang, R., & Zhou, Y. (2016). Hydrothermal formation of graphene aerogel for oil sorption: the role of reducing agent, reaction time and temperature. New Journal of Chemistry, 40(4), 3040-3046. https://doi.org/10.1039/c5nj03086b

[31] Trembecka-Wójciga, K., Sobczak, J., & Sobczak, N. (2023). A comprehensive review of graphene-based aerogels for biomedical applications. The impact of synthesis parameters onto material microstructure and porosity. Archives of Civil and Mechanical Engineering, 23(2). https://doi.org/10.1007/s43452-023-00650-6

[32] Gao, C., Zeliang, D., Hao, X., Yao, Y. L., & Guo, S. (2020). Preparation of reduced graphene oxide Aerogel and its adsorption for PB(II). ACS Omega, 5(17), 9903-9911. https://doi.org/10.1021/acsomega.0c00183

[33] Konuk, O. P., Alsuhile, A. A. A. M., Yousefzadeh, H., Ülker, Z., Bozbağ, S. E., García-González, C. A., Смирнова, И., & Erkey, C. (2023). The effect of synthesis conditions and process parameters on Aerogel properties. Frontiers in Chemistry, 11. https://doi.org/10.3389/fchem.2023.1294520

[34] Plata-Gryl, M., Castro-Muñoz, R., & Boczkaj, G. (2023). Chemically reduced graphene oxide based aerogels - insight on the surface and textural functionalities dependent on handling the synthesis factors. Colloids and Surfaces A: Physicochemical and Engineering Aspects, 675, 132005. https://doi.org/10.1016/j.colsurfa.2023.132005

[35] Geng, H., Liu, X., Shi, G., Bai, G., Ma, J., Chen, J., Wu, Z., Song, Y., Fang, H., & Wang, J. (2016). Graphene oxide restricts growth and recrystallization of ice crystals. Angewandte Chemie International Edition, 56(4), 997-1001. https://doi.org/10.1002/anie.201609230

[36] Guo, Q., Chen, S., Liu, Z., Yan, J., & Liu, H. (2022). Preparation and performance evaluation of graphene/hydroxypropyl methylcellulose composite aerogel for high viscosity oil adsorption. Journal of Environmental Chemical Engineering, 10(5), 108312. https://doi.org/10.1016/j.jece.2022.108312

[37] Fasina, O. O., & Colley, Z. (2008). Viscosity and Specific Heat of Vegetable Oils as a Function of Temperature: 35°C to 180°C. In International Journal of Food Properties (Vol. 11, Issue 4, pp. 738–746). Informa UK Limited. https://doi.org/10.1080/10942910701586273

[38] Canola oil Properties - Oklahoma State University. (2018, 1 décembre). https://extension.okstate.edu/fact-sheets/canola-oil-properties.html

[39] Peri, C. (2014). The Extra-Virgin Olive Oil Handbook. Wiley eBooks. https://doi.org/10.1002/9781118460412

[40] Viscosity of engine oil – Viscosity table and viscosity Chart | Anton Paar Wiki. (s. d.). Anton Paar. https://wiki.anton-paar.com/en/engine-oil/

[41] Groß, J., & Fricke, J. (1995). Thermal expansion of carbon and silica aerogels above room temperature. Journal of Non-Crystalline Solids, 186, 301-308. https://doi.org/10.1016/0022-3093(95)00053-4

[42] Xiao, J., Lv, W., Song, Y., & Zheng, Q. (2018). Graphene/Nanofiber aerogels : performance regulation towards multiple applications in dye adsorption and oil/water separation. Chemical Engineering Journal, 338, 202-210. https://doi.org/10.1016/j.cej.2017.12.156

[43] Liang, C., Du, R., Zhang, J., & Yi, T. (2015). Density controlled oil uptake and beyond: from carbon nanotubes to graphene nanoribbon aerogels. Journal of materials chemistry. A, Materials for energy and sustainability, 3(41), 20547-20553. https://doi.org/10.1039/c5ta04370k

[44] Buist, I., Potter, S., Newed, T., Mullin, J., 2011. Herding surfactants to contract and thicken oil spills in pack ice for in situ burning. Cold Regions Sci. Technol. 67 (1e2), 3e23.

[45] Kapoor, S., Rawat, H.S., 1994. Indian West coast spills: a remedial preparedness. Paper Number SPE 27157. Presented at Society of Petroleum Engineering Health, Safety and Environment in Oil and Gas Exploration and Production Conference, 25e27 January 1994, Jakarta, Indonesia.

[46] Adebajo, M.O., Frost, R.L., Kloprogge, J.T., Carmody, O., 2003. Porous materials for oil spill cleanup: a review of synthesis and absorbing properties. J. Porous Mater. 10 (3), 159e170.